Geometry and evolution of a fault-bend fold: Mount Bertha anticline

William Jamison
Alasdaire Pope*
Centre for Earth Resources Research, Department of Earth Sciences, Memorial University of Newfoundland, St. John's, Newfoundland A1B 3X5, Canada

ABSTRACT

Mount Bertha anticline is a major thrust-associated fold in the Rocky Mountains of western Canada, well displayed in a 900-m-thick middle Paleozoic carbonate sequence that forms the core of the fold. This carbonate sequence may be divided into three mechanical-stratigraphic units of roughly similar thicknesses: a lower, massive dolostone; a middle, layered dolostone; and an upper, micritic limestone. Substantial variations in structural geometry occur along strike. These variations correlate with changes in the thickness of the lower dolostone unit in the core of the fold that result from an oblique hanging-wall ramp.

A mode I fault-bend fold develops along most of the exposed strike length of Mount Bertha anticline. This configuration corresponds to regions where a full thickness of the lower dolostone unit occurs in the core of the fold. Where the lower dolostone unit is thin or absent in the hanging wall of the Mount Bertha thrust, the configuration of Mount Bertha anticline is dominated by second-order fault-propagation and detachment folds developed in the upper two mechanical-stratigraphic units. Along the length of the Mount Bertha structure, the limestone unit has been progressively attenuated and/or faulted in the lower forelimb region and overridden by the advancing thrust sheet.

The fold geometry of the central part of Mount Bertha anticline compares favorably with geometric models of fault-bend fold structures that allow forelimb thinning, except for parts of the fold affected by the tectonic removal of rock from the lower forelimb. Existing geometric models of fault-bend folds do not consider this process. A companion fold within the hanging wall of the Mount Bertha thrust, Cranswick anticline, is interpreted to be a mode I fault-bend fold that has been significantly modified by second-order fault-propagation folding during the waning phases of movement along the Mount Bertha thrust.

INTRODUCTION

John L. Rich (1934) proposed that the hanging-wall anticline of the Pine Mountain overthrust formed as the thrust sheet moved over the ramp region of the thrust (Fig. 1). The fault ramp formed prior to the folding and fundamentally controlled the fold shape. Although other workers have suggested that folding predates ramp formation (e.g., Willis, 1890) or is synchronous with it (e.g., Faill, 1973), the Rich model has remained a central paradigm for the interpretation of fold development in many thrust belts (Bally et al., 1966; Dixon, 1982; Suppe, 1980).

The geometric relationships between hanging-wall configuration and fault geometry was formalized by Suppe (1983), who introduced the term *fault-bend fold* for this particular fold-thrust style. Within the last decade, this and other fold-thrust models (e.g., Jamison, 1987; Suppe and Medwedeff, 1990; Chester and Chester, 1990; Mitra, 1990) have become common features in cross-section interpretations of fold-and-thrust systems. Despite the common appearance of the fault-bend fold geometry in cross sections based on convincing seismic and/or borehole data, clear examples of large-scale fault-bend folds in outcrop are uncommon. Outcrops that do exist typically display only a relatively small part of the fold structure. Included in this latter category is the Pine Mountain structure, which stimulated Rich's (1934) model.

Mount Bertha anticline provides an exceptionally complete exposure of a fault-

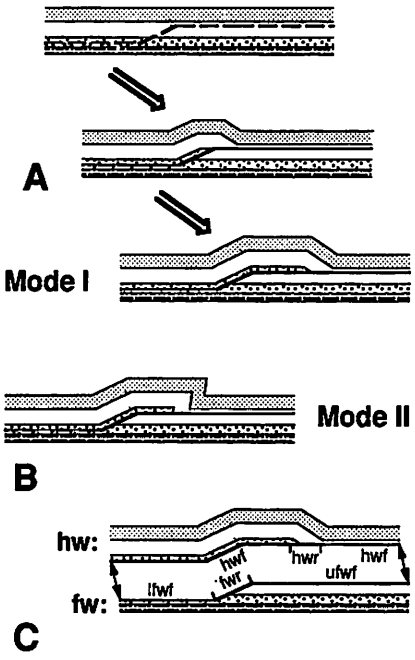

Figure 1. (A) The Rich (1934) or fault-bend fold concept for fold development in the hanging wall of a thrust. The thrust has a flat-ramp-flat geometry, and the fault surface forms prior to any significant fold development. The hanging-wall anticline develops as the hanging wall moves over the footwall ramp of the thrust. There are two geometrically viable fault-bend fold geometries for any specified ramp angle and bedding thickness change, namely the very open mode I geometry and a tighter mode II geometry (B) (Suppe, 1983; Jamison, 1987). (C) The fault surface may be subdivided with respect to the ramp region, with different subdivisions relating to the hanging wall (hw) vs. the footwall (fw): hwf, hanging-wall flat; hwr, hanging-wall ramp; lfwf, lower footwall flat; fwr, footwall ramp; ufwf, upper footwall flat.

*Present address: RTZ Mining and Exploration Ltd., Agencia Chile, Copiapo, Chile.

GSA Bulletin; February 1996; v. 108; no. 2; p. 208–224; 15 figures.

Pigg, K. B., and Trivett, M. L., 1994, Evolution of the glossopterid gymnosperms from Permian Gondwana: Journal of Plant Research, v. 107, p. 461–477.

Pigg, K. B., Davis, W. C., and Ash, S., 1993, A new permineralized Upper Triassic flora from the Petrified Forest National Park, Arizona: A preliminary report, *in* Lucas, S. G., and Morales, M., eds., The non-marine Triassic: New Mexico Museum of Natural History and Science Bulletin 3, p. 411–413.

Pittman, E. F., 1913, The coal measures of New South Wales, *in* McInnes, W. W., Dowling, D. B., and Leach, W. W., eds., The coal resources of the world: Toronto, Morang, v. 1, p. 3–14.

Raup, D. M., 1979, Size of the Permo–Triassic bottleneck and its evolutionary implications: Science, v. 206, p. 217–218.

Raymond, A., and Phillips, T. L., 1983, Evidence for an Upper Carboniferous mangrove community, *in* Teas, H. J., ed., Tasks for vegetation science: The Hague, Netherlands, Junk, v. 8, p. 19–30.

Renne, P. R., and Basu, A. R., 1991, Rapid eruption of the Siberian traps flood basalts at the Permo-Triassic boundary: Science, v. 253, p. 176–177.

Renne, P. R., Zhang, I. C., Richards, M. A., Black, M. T., and Basu, A. R., 1995, Synchrony and causal relations between Permian–Triassic boundary crisis and Siberian volcanism: Science, v. 269, p. 1413–1416.

Retallack, G. J., 1975, The life and times of a Triassic lycopod: Alcheringa, v. 1, p. 3–29.

Retallack, G. J., 1976, Triassic palaeosols in the upper Narrabeen Group of New South Wales. Part I. Features of the paleosols: Geological Society of Australia Journal, v. 23, p. 383–399.

Retallack, G. J., 1977a, Triassic palaeosols in the upper Narrabeen Group of New South Wales. Part II. Classification and reconstruction: Geological Society of Australia Journal, v. 24, p. 19–35.

Retallack, G. J., 1977b, Reconstructing Triassic vegetation of eastern Australia: A new approach to the biostratigraphy of Gondwanaland: Alcheringa, v. 1, p. 253–283.

Retallack, G. J., 1979, Middle Triassic coastal outwash plain deposits in Tank Gully, Canterbury: Royal Society of New Zealand Journal, v. 9, p. 397–414.

Retallack, G. J., 1980, Late Carboniferous to Middle Triassic megafossil floras from the Sydney Basin, *in* Herbert, C., and Helby, R., eds., A guide to the Sydney Basin: Geological Survey of New South Wales Bulletin 26, p. 384–430.

Retallack, G. J., 1990, Soils of the past: London, Unwin-Hyman, 520 p.

Retallack, G. J., 1991, Untangling the effects of burial alteration and ancient soil formation: Annual Reviews of Earth and Planetary Science, v. 19, p. 183–206.

Retallack, G. J., 1994, A pedotype approach to latest Cretaceous and earliest Tertiary paleosols in eastern Montana: Geological Society of America Bulletin, v. 106, p. 1377–1397.

Retallack, G. J., 1995, Permian–Triassic life crisis on land: Science, v. 267, p. 77–80.

Retallack, G. J., and Dilcher, D. L., 1981, A coastal hypothesis for the dispersal and rise to dominance of flowering plants, *in* Niklas, K. J., ed., Paleobotany, paleoecology and evolution: New York, Praeger, v. 2, p. 27–77.

Retallack, G. J., and Ryburn, R. J., 1982, Middle Triassic deltaic deposits in Long Gully, near Otematata, north Otago, New Zealand: Royal Society of New Zealand Journal, v. 12, p. 207–217.

Retallack, G. J., Gould, R. E., and Runnegar, B., 1977, Isotopic dating of a Middle Triassic megafossil flora from near Nymboida, northeastern New South Wales: Linnaean Society of New South Wales Proceedings, v. 101, p. 77–113.

Retallack, G. J., Renne, P. R., and Kimbrough, D. L., 1993, New radiometric ages for Triassic floras of southeast Gondwana, *in* Lucas, S. G., and Morales, M., eds., The non-marine Triassic: New Mexico Museum of Natural History and Science Bulletin 3, p. 415–418.

Robinson, J. M., 1990, Lignin, land plants and fungi: Biological evolution affecting Phanerozoic oxygen balance: Geology, v. 15, p. 607–610.

Ross, C. A., and Ross, J. R. P., 1988, Late Paleozoic transgressive-regressive deposition: Society of Economic Paleontologists and Mineralogists Special Paper 42, p. 227–247.

Sahni, B., 1932, A petrified *Williamsonia* from the Rajmahal Hills, India: Memoir of the Geological Survey of India, Palaeontologia Indica, v. 20, p. 1–19.

Sahni, B., 1948, The Pentoxyleae—A new group of Jurassic gymnosperms from the Rajmahal Hills of India: Botanical Gazette, v. 110, p. 47–80.

Scheckler, S. E., 1986, Geology, floristics and paleoecology of Late Devonian coal swamps from Appalachian Laurentia (U.S.A.): Annales de la Societè Gèologique de Belgique, v. 109, p. 209–222.

Schneider, W., 1990, Floral successions in Miocene bogs of central Europe, *in* Knobloch, E., and Kvaček, Z., eds., Proceedings of the Symposium on Paleofloristic and Paleoclimatic Changes in the Cretaceous and Tertiary: Prague, Geological Survey, p. 203–214.

Schubert, J. K., and Bottjer, D. J., 1992, Early Triassic stromatolites as post–mass extinction disaster forms: Geology, v. 20, p. 883–886.

Scotese, C. R., and Denham, C. R., 1988, Terra mobilis: Plate tectonics for the Macintosh: Austin, Texas, Earth in Motion Technologies (software).

Sereno, P. C., Forster, C. A., Rogers, R. R., and Monetta, A. M., 1993, Primitive dinosaur skeleton from Argentina and the early evolution of Dinosauria: Nature, v. 361, p. 64–66.

Shearer, J. C., Staub, J. R., and Moore, T. A., 1994, The conundrum of coal bed thickness: A theory for stacked mire sequences: Journal of Geology, v. 102, p. 611–617.

Smyth, M., 1980, Thick coal members: Products of an inflationary environment? Australian Coal Geology, v. 2, p. 53–76.

Spicer, R. A., and Chapman, J. L., 1990, Climate change and the evolution of high latitude terrestrial vegetation and floras: Trends in Ecology and Evolution, v. 5, p. 279–284.

Stanley, G. D., 1992, Tropical reef ecosystems and their evolution, *in* Nierenberg, W. A., ed., Encyclopedia of earth system science: San Diego, California, Academic Press, v. 4, p. 375–388.

Steel, R. J., 1974, Cornstone (fossil caliche)—Its origin, stratigraphic and sedimentological importance in the New Red Sandstone, Scotland: Journal of Geology, v. 82, p. 351–369.

Stockey, R. A., 1983, *Pinus driftwoodensis* sp. n. from the early Tertiary of British Columbia: Botanical Gazette, v. 144, p. 148–156.

Stockey, R. A., 1984, Middle Eocene *Pinus* remains from British Columbia: Botanical Gazette, v. 145, p. 262–274.

Stockey, R. A., 1987, A permineralized flower from the middle Eocene of British Columbia, Canada: American Journal of Botany, v. 74, p. 1878–1887.

Stockey, R. A., and Pigg, K. B., 1991, Flowers and fruits of *Princetonia allenbyensis* (Magnoliopsida, family indet.) from the middle Eocene Princeton chert of British Columbia: Reviews of Palaeobotany and Palynology, v. 70, p. 163–172.

Stricker, G. D., 1991, Economic Alaskan coal deposits, *in* Gluskoter, H. J., Rice, D. D., and Taylor, R. B., eds., Economic geology, U.S.: Geological Society of America, Geology of North America, v. P-2, p. 591–601.

Stubblefield, S. F., and Taylor, T. N., 1988, Recent advances in palaeomycology: New Phytologist, v. 108, p. 3–25.

Suescún-Gomez, D., 1978, Coal deposits in Colombia, *in* Kottlowski, F. E., Cross, A. T., and Meyerhoff, A. A., eds., Coal resources of the Americas: Geological Society of America Special Paper 179, p. 49–56.

Taylor, E. L., and Taylor, T. N., 1990, Structurally preserved Permian and Triassic floras from Antarctica, *in* Taylor, T. N., and Taylor, E. L., eds., Antarctic paleobiology: New York, Springer, p. 149–163.

Taylor, E. L., and Taylor, T. N., 1993, Fossil tree rings and paleoclimate from the Triassic of Antarctica, *in* Lucas, S. G., and Morales, M., eds., The non-marine Triassic: New Mexico Museum of Natural History and Science Bulletin 3, p. 453–455.

Taylor, E. L., Taylor, T. N., and Collinson, J. W., 1989, Depositional setting and paleobotany of Permian and Triassic permineralized peats from the central Transantarctic Mountains, Antarctica: International Journal of Coal Geology, v. 12, p. 20–27.

Taylor, E. L., Taylor, T. N., and Cuneo, R. N., 1990, The present is not the key to the past: A polar forest from the Permian of Antarctica: Science, v. 257, p. 1675–1677.

Taylor, T. N., Taylor, E. L., and Del Fueyo, G., 1993, Permineralized Triassic plants from Antarctica, *in* Lucas, S. G., and Morales, M., eds., The non-marine Triassic: New Mexico Museum of Natural History and Science Bulletin 3, p. 149–163.

Tidwell, W. D., Kim, J.-H., and Kimura, T., 1987, Mid-Mesozoic leaves from near Ida Bay, southern Tasmania, Australia: Royal Society of Tasmania Papers and Proceedings, v. 121, p. 159–167.

Vakhrameev, V. A., Dobruskina, I. A., Meyen, S. V., and Zaklinskaya, E. D., 1978, Paläozoische und mesozoische Floren Eurasiens und die Phytogeographie dieser Zeit: Jena, West Germany, G. Fischer, 300 p.

Veevers, J. J., 1989, Middle/Late Triassic (230 ± 5 Ma) singularity in the stratigraphic and magmatic history of the Pangean heat anomaly: Geology, v. 17, p. 784–787.

Veevers, J. J., 1990a, Tectonic-climatic supercycles in the billion year plate-tectonic eon: Permian Pangean icehouse alternates with Cretaceous dispersed-continents greenhouse: Sedimentary Geology, v. 68, p. 1–16.

Veevers, J. J., 1990b, Development of Australia's post-Carboniferous sedimentary basins: Australian Petroleum Exploration Association Journal, v. 16, p. 25–32.

Veevers, J. J., 1994, Pangea: Evolution of a supercontinent and its consequences for Earth's paleoclimate and sedimentary environments, *in* Klein, G. de V., ed., Pangea: Paleoclimate, tectonics, and sedimentation during accretion, zenith and breakup of a supercontinent: Geological Society of America Special Paper 288, p. 13–23.

Veevers, J. J., and Tewari, R. C., 1995, Gondwana master basin of peninsular India between Tethys and the interior of the Gondwanaland province of Pangea: Geological Society of America Memoir 187 (in press).

Veevers, J. J., Conaghan, P. J., and Shaw, S. E., 1994a, Turning point in Pangean environmental history of the Permo-Triassic (P-Tr) boundary, *in* Klein, G. de V., ed., Pangea: Paleoclimate, tectonics, and sedimentation during accretion, zenith and breakup of a supercontinent: Geological Society of America Special Paper 288, p. 187–196.

Veevers, J. J., Powell, C. McA., Collinson, J. W., and López-Gamundí, O. R., 1994b, Synthesis, *in* Veevers, J. J., and Powell, C. McA., eds., Permian–Triassic basins and foldbelts along the Panthalassan margin of Gondwanaland: Geological Society of America Memoir 184, p. 331–353.

Visscher, H., and Brugman, W. A., 1988, The Permian-Triassic boundary in the southern Alps: A palynological approach, *in* Cassinis, G., ed., Permian and Triassic boundary in the South Alpine segment of the western Tethys: Proceedings of a conference and additional reports: Memorie della Societa Geologica Italiana, v. 34, p. 121–128.

Wang, K., Geldsetzer, H. H. J., and Krouse, H. R., 1994, Permian–Triassic extinction: Organic $\delta^{13}C$ evidence from British Columbia, Canada: Geology, v. 22, p. 580–584.

Wang, Z., 1993, Evolutionary ecosystem of Permo–Triassic red beds in north China: A historic record of global desertification, *in* Lucas, S. G., and Morales, M., eds., The non-marine Triassic: New Mexico Museum of Natural History and Science Bulletin 3, p. 471–476.

Webb, J. A., and Fielding, C. R., 1993, Permo–Triassic sedimentation within the Lambert Graben, northern Prince Charles Mountains, East Antarctica, *in* Findlay, R. H., Unrug, R., Banks, M. R., and Veevers, J. J., eds., Gondwana Eight: Proceedings of the Eighth Gondwana Symposium, Hobart: Rotterdam, Netherlands, A. A. Balkema, p. 357–369.

Weber, K. I., 1993, Paleosols in Triassic sediments of southeast Germany, *in* Lucas, S. G., and Morales, M., eds., The non-marine Triassic: New Mexico Museum of Natural History and Science Bulletin 3, p. 477–478.

Wen S.-X., Zhang B.-G., Wang Y.-G., Sun D.-L., Wang Y.-J., Chen C.-Z., Dong D.-Y., Liao W.-H., Chen T.-E., He G.-X., Mu X.-N., Yin J.-X., and Wu H.-R., 1981, Sedimentary development and formation of stratigraphic region in Xizang, *in* Liu D.-S., ed., Geological and ecological studies of Qinghai-Xizang Plateau: Beijing, Science Press, and New York, Gordon and Breach, v. 1, p. 119–130.

White, M. E., 1991, Time in our hands: Balgowlah, New South Wales, Reed, 191 p.

Wilson, R. L., 1975, Capella district, *in* Traves, D. M., and King, D., eds., Economic geology of Australia and New Zealand: Australasian Institute of Mining and Metallurgy Monograph 6, p. 78–82.

Wood, R., 1993, Nutrients, predation and the history of reef-building: Palaios, v. 8, p. 526–543.

Worsley, T. R., Moore, T. L., Fraticelli, C. M., and Scotese, C. R., 1994, Phanerozoic CO_2 levels and global temperatures inferred from changing paleogeography, *in* Klein, G. de V., ed., Pangea: Paleoclimate, tectonics and sedimentation during accretion, zenith and breakup of a supercontinent: Geological Society of America Special Paper 288, p. 57–74.

Wu C.-L., Li S.-T., and Cheng S.-T, 1992, Humid-type alluvial fan deposits and associated coal seams in the Lower Cretaceous Haizhou Formation, Fuxin Basin of northeastern China, *in* McCabe, P. J., and Parrish, J. T., eds., Controls on the distribution and quality of Cretaceous coals: Geological Society of America Special Publication 267, p. 269–286.

Yang Z. Y., Chen Y. Q., and Wang H. Z., 1986, The geology of China: New York, Oxford University Press, 303 p.

Zahnle, K. J., 1990, Atmospheric chemistry by large impacts, *in* Sharpton, V. L., and Ward, P. D., eds., Global catastrophes in Earth history: Geological Society of America Special Paper 247, p. 271–300.

Ziegler, A. M., Scotese, C. R., McKerrow, W. S., Johnson, M. E., and Bambach, R. K., 1979, Paleozoic paleogeography: Annual Review of Earth and Planetary Science, v. 7, p. 473–502.

Ziegler, A. M., Scotese, C. R., and Barrett, S. F., 1983, Mesozoic and Cenozoic paleogeographic maps, *in* Brosche, P., and Sündermann, J., eds., Tidal friction and the Earth's rotation: Berlin, Springer-Verlag, p. 240–252.

Ziegler, A. M., Parrish, J. M., Yao Y.-P., Gyllenhall, E. D., Rowley, P. B., Parrish, J. T., Nie S.-Y., Bekker, A., and Hulver, M. L., 1993, Early Mesozoic phytogeography and climate: Philosophical Transactions of the Royal Society of London, v. B341, p. 297–305.

Ziegler, P. A., 1988, Evolution of the Arctic–North Atlantic and the Western Tethys: American Association of Petroleum Geologists Memoir 43, 198 p.

MANUSCRIPT RECEIVED BY THE SOCIETY OCTOBER 21, 1994
REVISED MANUSCRIPT RECEIVED JUNE 27, 1995
MANUSCRIPT ACCEPTED JUNE 30, 1995

Printed in U.S.A.

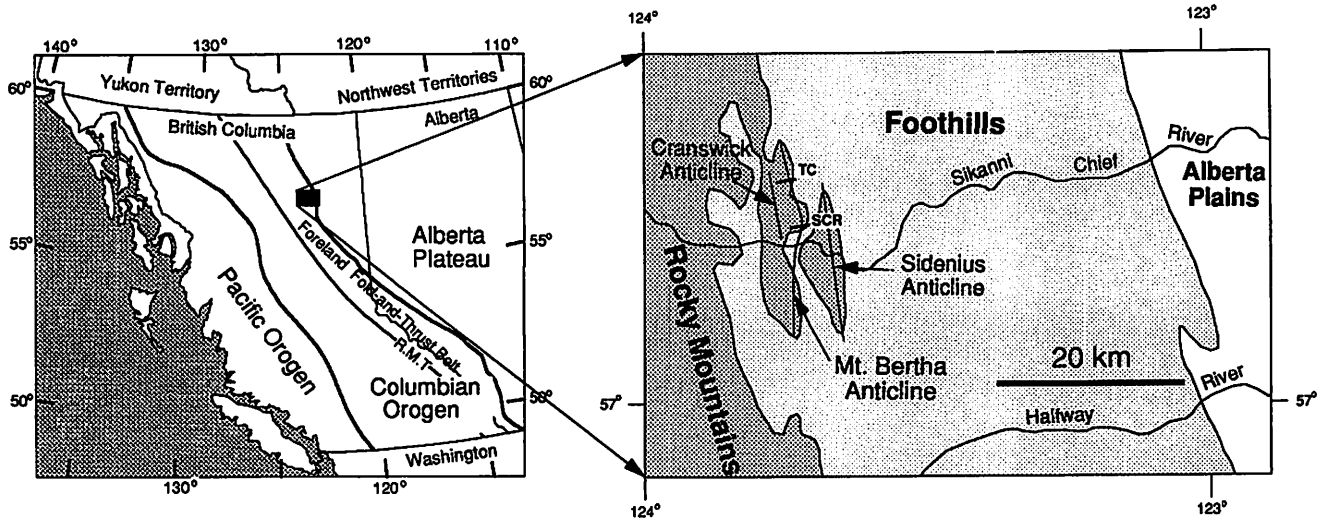

Figure 2. Location maps for the Mount Bertha study area. Structural subprovince designation of Thompson (1989) for northeastern British Columbia. R.M.T., Rocky Mountain Trench; SCR, Sikanni Chief River profile exposure (see Figs. 3A, 3B, and 5A); TC, Trimble Creek profile exposure (see Figs. 3C, 3D, and 5B).

bend fold (Figs. 2 and 3). This large, north-south–trending structure is located within the foreland fold-and-thrust belt region of the western Canadian Cordillera in northeastern British Columbia, Canada, at the eastern margin of the Rocky Mountain structural subprovince (Fig. 2). The Mount Bertha structure encompasses three mountains: the formally named Mount Bertha, and the informally named North Bertha and South Bertha. The trace of the Mount Bertha thrust follows the eastern margin of all three mountains for a strike distance of ~15 km. The Mount Bertha thrust carries two major anticlines. The eastern and larger of the two is Mount Bertha anticline; the western is Cranswick anticline.

Two transecting (east-west) drainages provide extremely good cross-sectional exposures of Mount Bertha anticline within middle Paleozoic carbonate rocks (Fig. 3). The broad fold overlying a planar thrust, as displayed along the Sikanni Chief River drainage (Figs. 3A and 3B), is the hanging-wall geometry predicted by the Rich-model (Rich, 1934) or mode I fault-bend fold (Suppe, 1983) form of thrust-associated folding. Five kilometers to the north, along the Trimble Creek drainage, this same anticlinal structure displays a much more complex configuration (Figs. 3C and 3D). This transition in structural configuration along strike might represent different stages or paths in the evolution of a fault-bend fold or, alternatively, changes in the fundamental fold-thrust style of the Mount Bertha structure.

We have examined the outcropping Mount Bertha structure in detail in an effort to (1) assess the nature and possible causes of the along-strike variation in structural geometry and (2) evaluate existing conceptual and geometric/kinematic models of fault-bend folding. Our primary database consists of a structural map and two profile sections of Mount Bertha anticline. These surface data form the basis for structural cross sections, structure-contour and hanging-wall cutoff maps of the Mount Bertha thrust, a general interpretation of the evolution of the Mount Bertha structure, and a critical evaluation of the formalized fault-bend fold models.

STRATIGRAPHY

The present exposure of the Mount Bertha structure includes seven formations (following the stratigraphic nomenclature of Taylor and MacKenzie, 1970) ranging from Silurian through Mississippian in age (Fig. 4). These several formations may be grouped into four distinct mechanical-stratigraphic units, namely a shale unit, a very fine grained limestone unit, a well-bedded, medium crystalline dolostone unit, and a massive, microcrystalline dolostone unit.

The youngest unit cropping out in the study area is the Middle Devonian through Mississippian Besa River Formation (MD_{br}), a black-weathering, calcareous to noncalcareous shale (Bamber et al., 1968). A complete section of the Besa River Formation is not present in the Mount Bertha area. Projecting from studies both to the north and the south (Bamber et al., 1968; Thompson, 1989), we estimate a stratigraphic thickness of ~650 m.

The Middle Devonian Slave Point, Sulfur Point, and Pine Point formations are components of a stromatoporoidal carbonate buildup (Taylor and MacKenzie, 1970). Through the Mount Bertha area, the Slave Point and Sulfur Point formations consist primarily of thin- to medium-bedded limestone, with local pods of secondary dolomite and chert. The contact between these two units is concordant in the Mount Bertha area. The Sulfur Point Formation is a lime mudstone, generally barren of fossils, and the overlying Slave Point Formation (lime mudstone to wackestone) contains variable fossil concentrations, primarily amphoporoids and stromatoporoids. Because we were not able to identify the boundary between these two formations in much of the study area, we have combined them for the purposes of our structural mapping. The composite limestone sequence is referred to as the Slave/Sulfur Point Formation (D_{sp}) and has a cumulative thickness of 220 m.

The Pine Point Formation (D_{pp}) is a fine- to medium-crystalline, thin- to medium-bedded, locally vuggy dolostone, 325 m thick in the central part of the study area. An erosional contact is evident between the Pine Point Formation and the overlying Slave/Sulfur Point Formation in the southern part of our study area. This results in some thinning (assumed small) of the Pine Point Formation southward along the Mount Bertha

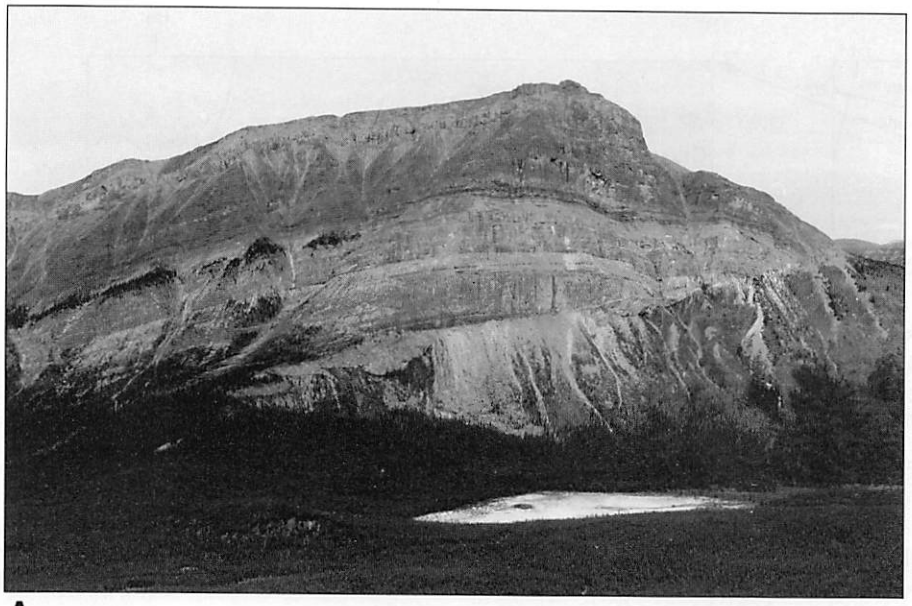

A

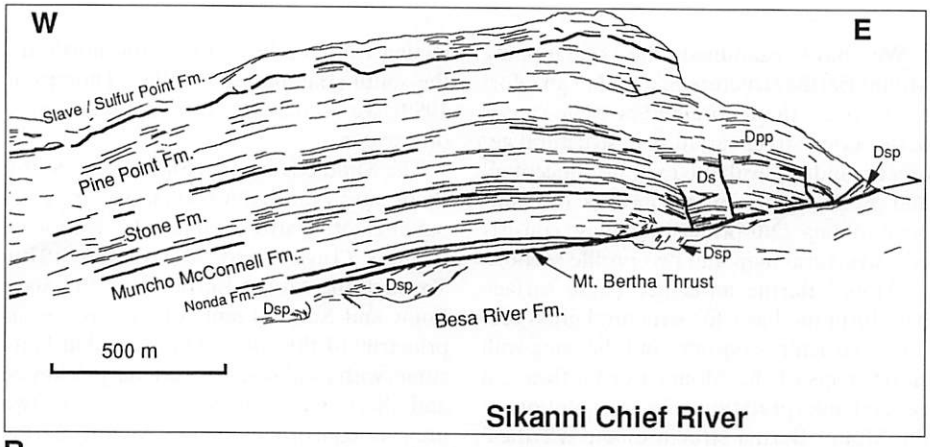

B

Figure 3. (A) Photograph and (B) line tracing of the profile exposure of Mount Bertha anticline on north side of Sikanni Chief River. (C) Photograph and (D) line tracing of the profile exposure of Mount Bertha anticline on north side of Trimble Creek. Dsp, Slave/Sulfur Point Formation; Dpp, Pine Point Formation; Ds, Stone Formation. All views are northward along the structural axis of Mount Bertha anticline. See Figures 2 and 6 for location of exposures and Figure 4 for stratigraphic column.

structure. The contact between the Pine Point Formation and the underlying Stone Formation is concordant.

The Late Silurian to Middle Devonian (estimated age; Thompson, 1989) Stone Formation (D_s) and Muncho-McConnell Formation (SD_m) are dense, nonfossiliferous, very fine grained to microcrystalline dolostone units, with thicknesses of 200 m and 120 m, respectively. Both formations commonly form massive outcrops and steep cliff faces. All contacts of these two formations are concordant.

The oldest formation cropping out in the Mount Bertha area is the Silurian Nonda Formation (S_n), a fine-crystalline dolostone. Although the Nonda Formation is several hundred meters thick in the region, a maximum of ~50 m of the upper part of this formation is exposed in the Mount Bertha structure.

STRUCTURAL PROFILES: MOUNT BERTHA ANTICLINE

The general structural configuration of Mount Bertha anticline as seen in the profile exposures along the north slopes of the Sikanni Chief River and Trimble Creek drainages (see Fig. 2) is rendered by tracings from photomosaics (Figs. 3B and 3D). The positions of 50 survey triangulation points have been determined on each exposure. Surveyed points projected parallel to the fold axis (π-pole) into a common profile plane (the structure is cylindrical throughout each exposure) are used to adjust the photomosaic tracings to true and accurate profile sections of Mount Bertha anticline (Fig. 5).

Sikanni Chief River Profile

In the Sikanni Chief River profile, Mount Bertha anticline is a broad fold with an interlimb angle of ~154 ° (Figs. 3A, 3B, and 5A). The Mount Bertha thrust broadly undulates across the profile, with a westward dip of ~14°. The Mount Bertha thrust cuts upsection in the hanging wall along strike both to the north and to the south from this location. As a result, the greatest stratigraphic thickness of middle Paleozoic carbonate rocks encountered in Mount Bertha anticline (~900 m) occurs in this section.

Beneath the backlimb of Mount Bertha anticline, the fault surface parallels bedding (S_0) in the hanging wall, that is, the fault is a hanging-wall flat through this part of the fold (see Fig. 5A). In the forelimb, hanging-wall strata are truncated against the fault through two separate hanging-wall ramps. One relatively short ramp cuts upsection from the upper Nonda Formation (S_n) to the upper Muncho-McConnell Formation (SD_m; total of ~130 m of section). A second ramp cuts upsection through the Stone (D_s), Pine Point (D_{pp}), and Slave/Sulfur Point (D_{sp}) formations and into the Besa River Formation (MD_{br}) shale. These two hanging-wall ramps are separated by a hanging-wall flat (approximate) in the upper SD_m dolostone. This secondary flat has a cross-strike length of ~400 m.

Within the D_s, SD_m, and S_n formations, the smooth, gentle flexure of beds across the fold is interrupted only by a few second-order extensional and contractional faults (meters to tens of meters displacement) in the hinge and forelimb and a zone of complex folding directly above the western hanging-wall ramp. (We use the term *second-order* to distinguish features that are macroscale but small compared to the major structures of the region, such as Mount Bertha anticline.) Broad bedding undulations are evident in the D_{sp} limestone throughout the backlimb and hinge region of the fold (Figs. 3A, 3B, and 5A), but it is unclear whether these are sedimentary or structural features. At the eastern end of this profile, a

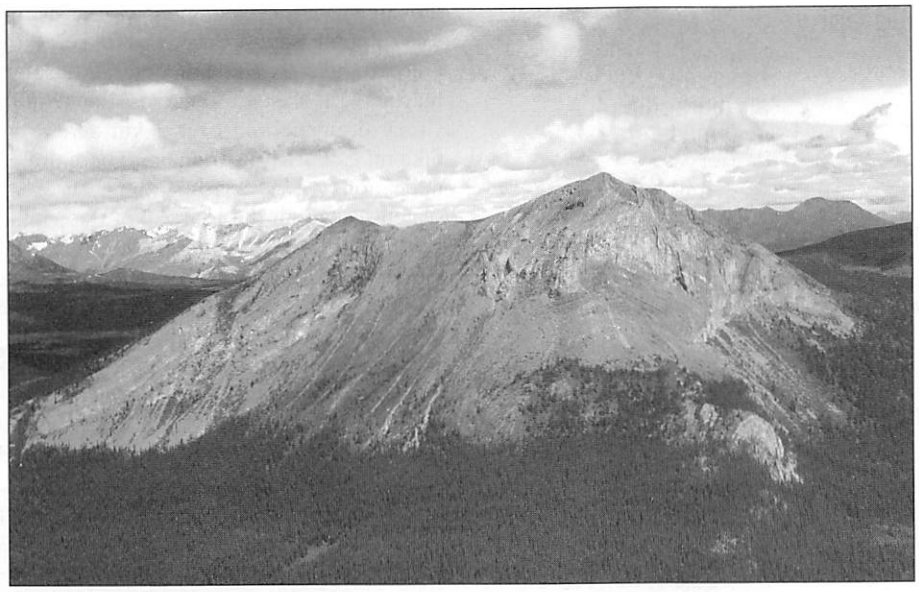

C

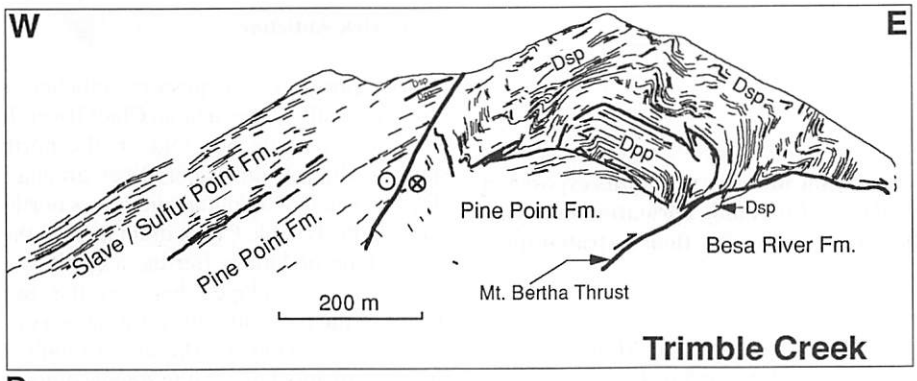

D

Figure 3. (*Continued*).

horse or imbricate slice of the Mount Bertha thrust contains overturned beds of D_{sp} limestone. The upper bounding fault for this horse dies out into S_0 in the D_{sp} limestone within 1 km along strike to the north.

Two major carbonate lozenges are evident in the footwall of the Mount Bertha thrust in the Sikanni Chief River profile, in direct contact with the fault surface (Figs. 3A, 3B, and 10A, below). These are both overturned blocks of D_{sp} limestone, very similar in appearance to the fault-bounded D_{sp} limestone at the eastern end of this profile. D_{sp} limestone is, in fact, found continuously along the fault in this profile section. The larger blocks of limestone in the fault zone are connected by a zone of strongly tectonized limestone only a few meters wide. A cataclasite zone ~5 cm to 1 m thick is developed along the contact between the fault zone limestone and the hanging-wall dolostone. The contact between the fault zone limestone and the underlying MD_{br} shale is certainly tectonic, but no shear fabric is developed.

The structurally thinned D_{sp} limestone in the lower forelimb can be followed into the subthrust limestones. It is our interpretation that the limestone beds in the lower forelimb have been, progressively, overturned, attenuated, and finally overridden by the advancing thrust sheet. The result is a recumbent fold geometry in the D_{sp} limestone (with a highly attenuated and irregular overturned limb) that encases a fault-bend fold geometry in the dolostone units.

Trimble Creek Profile

On the south face of North Bertha, Mount Bertha anticline is well exposed in the D_{pp} dolostone and D_{sp} limestone (Figs. 3C, 3D, and 5B). Uppermost D_s dolostone is inferred to occur in the core of the fold (Fig. 5B) based on exposures in the Trimble Creek valley. The Mount Bertha thrust fault is exposed only beneath the forelimb and core of the fold. The hanging-wall flat beneath the backlimb of Mount Bertha anticline is ~300 m higher in the stratigraphic section here than in the Sikanni Chief River profile, which is 5 km south.

The core and forelimb of Mount Bertha anticline in this profile section is a zone of complex, second-order folding in the D_{sp} limestone and second-order fold-and-thrust deformation in the D_{pp} dolostone. The definition of a single anticlinal structure is really only approximated by the enveloping surface of this fold complex. The core/forelimb region is separated from a homoclinally dipping backlimb by a steeply dipping fault with ~100 m reverse dip separation in this profile section (Fig. 5B). Kinematic indicators along exposures of this fault (the North Bertha strike-slip fault) to the north consistently indicate or agree with sinistral strike slip (horizontal slickensides, mesoscale Riedel shears, and minor folds).

The box fold developed within the Pine Point Formation in the core of Mount Bertha anticline is a fault-propagation fold associated with a second-order backthrust that emanates from an inflection in the Mount Bertha thrust surface. This and the other second-order faults in the Pine Point Formation consistently die out into folds in the lower part of the D_{sp} limestone. A marked disharmony exists between these structures within the D_{pp} dolostone and the folds in the overlying D_{sp} limestone. The D_{sp} limestone folds are detachment or lift-off folds formed above a detachment surface lying very close to the limestone-dolostone (D_{sp}-D_{pp}) boundary. Considerable structural attenuation occurs in the limbs of the limestone folds, especially the steep to overturned forelimbs.

The easternmost of the second-order folds in the D_{sp} limestone has an axial surface that aligns downdip with a planar segment of the Mount Bertha thrust (see Figs. 3D and 5B). The thrust itself has a distinct inflection at the point of intersection with this fold axial surface, and the fault dips eastward beneath the forelimb of this fold. We speculate that, if the hanging wall were to have advanced, this east-dipping segment of the Mount Bertha thrust would have become inactive and the main fault would have shifted to a new location along the axial surface of this second-order fold, akin to the model of Al Saffar (1993). The forelimb region of this particular second-order fold would, consequently, become detached

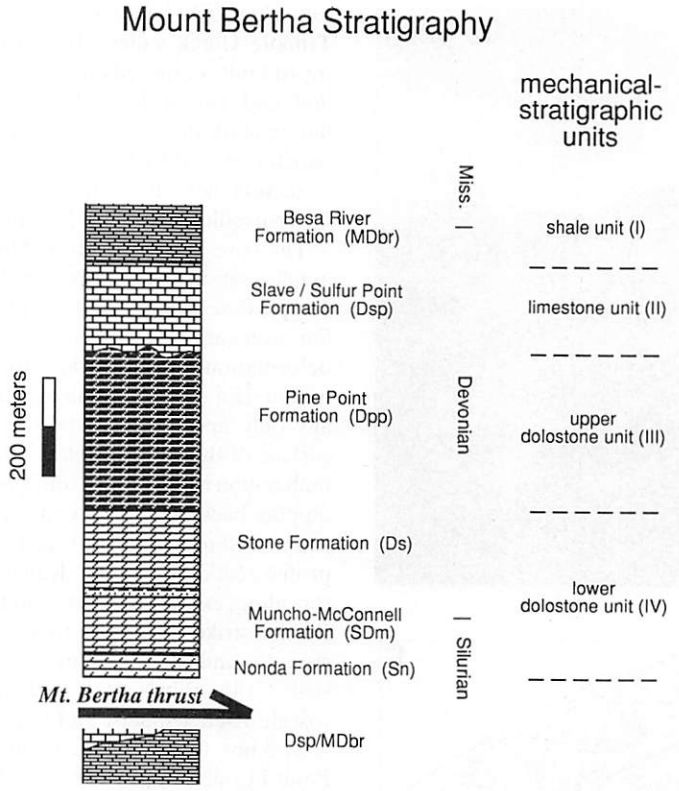

Figure 4. Lithostratigraphy and mechanical-stratigraphic units for rock units exposed in the Mount Bertha study area. The indication of Slave/Sulfur Point Formation overlying Besa River Formation beneath the thrust reflects a structural rather than a stratigraphic relationship, as discussed later in the text.

from the hanging wall of the structure and remain as a large pod of limestone subjacent to the Mount Bertha thrust surface.

MAP EXPRESSION

Mount Bertha Anticline

The π-plots of S_0 (bedding) and S_1 (cleavage) indicate Mount Bertha anticline has a fold axis (π-pole) that is subhorizontal and trends 350° ± 10° throughout South Bertha and Mount Bertha (Fig. 6). Through the southern part of North Bertha the fold axis shifts to a trend of 335°, then returns to a more northerly orientation in the northern part of the study area. Slickensides and lineations on L-S tectonites within or near the Mount Bertha thrust fault zone indicate a transport direction perpendicular to the local π-pole.

Along South Bertha, Mount Bertha anticline is a very open fold with no evidence of second-order structures. On the southern slopes of Mount Bertha, the forelimb of Mount Bertha anticline displays broad undulations (Figs. 3A and 3B) that, northward along the eastern flank of Mount Bertha, become distinct, second-order box folds involving the D_{pp} dolostone and D_{sp} limestone (Figs. 6 and 7). These are similar to the second-order folds that dominate the structural expression of Mount Bertha anticline on the south flank of North Bertha (Figs. 3C, 3D, and 5B) and persist along the length of North Bertha (Fig. 6).

The second-order folds in the D_{sp} limestone on North Bertha generally have wavelengths of 100–200 m and an axial length of <1 km. The overall structural trend of Mount Bertha anticline on North Bertha is almost due north, but these second-order folds individually trend north-northwest, plunge in one or both directions, and are crudely arranged in a right-stepping en echelon array (Fig. 6). The sinistral North Bertha strike-slip fault strikes 350° and separates a homoclinally dipping backlimb from the complexly folded core and forelimb region of the fold (see Fig. 5B) along the entire length of North Bertha (Fig. 6). This strike-slip fault is not present on the south side of Trimble Creek.

In general form, Mount Bertha anticline has an open fold geometry with a steeply west-dipping axial surface. The fold crest (at any particular stratigraphic level) is offset, in map view, at least 0.5 km across the Trimble Creek drainage and over 1 km across the Sikanni Chief River drainage. There are no indications of a corresponding offset on structures within the footwall of the Mount Bertha thrust within these drainages. Second-order folds and faults in the Trimble Creek profile section produce much more fault-parallel shortening within the hanging-wall sheet than do the hanging-wall structures in the Sikanni Chief River profile section (Fig. 5). The offset of the hanging-wall structure across Trimble Creek thus could be explained in part or in full by a difference in thrust-parallel shortening within Mount Bertha anticline across this drainage. This argument would not apply to the noted offset across the Sikanni Chief River drainage.

Cranswick Anticline

No expression of Cranswick anticline is observed south of the Sikanni Chief River. It is a low-amplitude box fold on the north slope of the Sikanni Chief River drainage (Fig. 8). The fold amplitude increases northward to the Trimble Creek drainage. On the north slope of Mount Bertha, a significant syncline has developed between the two hinges of the box fold, thus forming two distinct anticlines (Fig. 6). The western limb of the western anticline is quite steeply dipping (>60°). The two anticlinal hinges merge into a single hinge zone on the north side of the Trimble Creek drainage, but the steep dip of the west limb of the fold persists, resulting in a west-vergent fold asymmetry. Cranswick anticline dies out with a northward plunge at Cranswick Lake (Fig. 6). The π-plot of S_0 and S_1 indicates a cylindrical fold geometry along the entire length of this fold, with a π-pole orientation 2°→355°. There is no strike offset of Cranswick anticline across the Trimble Creek drainage.

Footwall to the Mount Bertha Thrust

The largest structure evident in the footwall of the Mount Bertha thrust is Sidenius anticline. It lies east of Mount Bertha anticline (see Fig. 2) and largely outside our mapping area. An intermediate-scale anticline cropping out in D_{sp} limestone is mapped directly beneath the Mount Bertha thrust in both the Sikanni Chief River and Trimble Creek drainages (Figs. 6 and 9). We presume this is a continuous structure

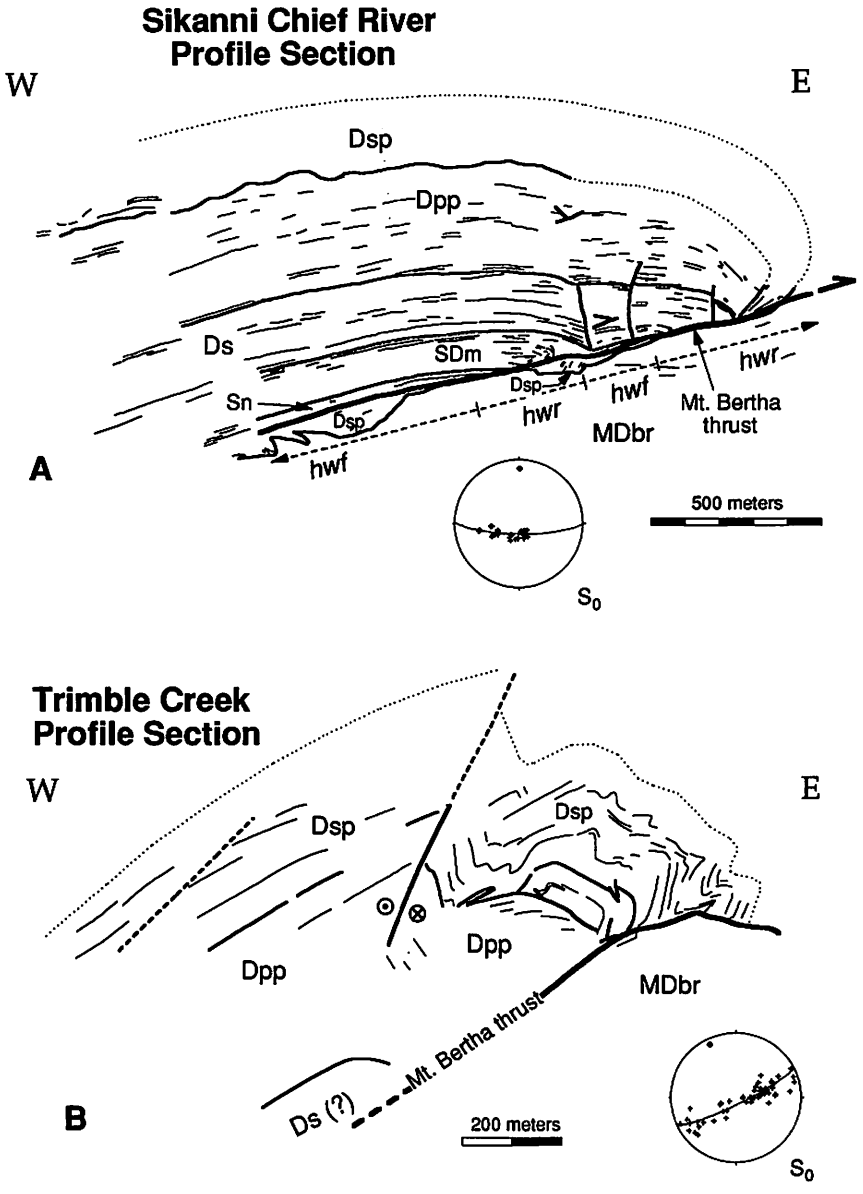

Figure 5. True profile sections of Mount Bertha anticline based on exposures and survey control points on north side of (A) Sikanni Chief River (see Figs. 3A and 3B) and (B) Trimble Creek (see Figs. 3C and 3D). Line of profile sections identified in Figures 6 and 11. *hwf*, hanging-wall flat; *hwr*, hanging-wall ramp (compare Fig. 1C). See Figure 4 for formation abbreviations.

(Camp anticline) between these two locations. Camp anticline has a much more strongly developed axial planar cleavage than do second-order D_{sp} folds of comparable size in the hanging wall of the Mount Bertha thrust (see Fig. 3C). Second-order thrusts that intercalate uppermost D_{sp} limestone with MD_{br} shale are common in the Sikanni Chief River drainage both east and west of Camp anticline.

MD_{br} shale is widespread but recessive in the footwall of the Mount Bertha thrust. Where the shale is involved in the second-order footwall faulting, it displays a moderate to strong cleavage, which usually obscures or transposes bedding. On the south slope of Mount Bertha, however, a relatively thick (~300 m) shale section beneath the Mount Bertha thrust has a gentle dip with broad undulations (see Fig. 3A).

CROSS-SECTION INTERPRETATIONS

Four cross-section interpretations of the Mount Bertha structure have been generated at strike intervals of ~4 km (Figs. 6 and 10). The lines of section (oriented 080°) are approximately orthogonal to the fold axes of both Mount Bertha anticline and Cranswick anticline. All sections are through areas with a relatively high density of measurement stations. In all cases, control of structural geometry is much better for the hanging wall of the Mount Bertha thrust than the footwall region. The position of Mount Bertha thrust beneath Mount Bertha anticline is well defined in outcrop near each of the cross sections. There is no subsurface control for these sections. Our interpretations extend only to the limits of our mapping. A broad valley (~3 km wide) of very little outcrop lies west of our map area. Taylor (1979) maps this as folded, but unfaulted, D_{br} shale. Cross section B–B′ (Fig. 10B) is the most highly controlled of the sections and provides a reference for the discussion of the other cross sections.

Central Bertha (B–B′). The base of the Sikanni Chief River drainage (~1200 m elevation) defines the lower limit of control for this section (Fig. 10B). The geometry of Mount Bertha anticline in this cross section is similar to the Sikanni Chief River profile (Fig. 5A), which is ~1 km south, except that here the intermediate hanging-wall flat in the Muncho-McConnell Formation is much broader. The line of section coincides with the cliff face exposure of Cranswick anticline (Fig. 8), which, here, is interpreted to be a fault-propagation fold developed above a broad hinge or inflection in the Mount Bertha thrust and superposed on a very broad, low-amplitude fault-bend fold.

In the footwall, Camp anticline is well defined in the D_{sp} limestone. The configuration of Sidenius anticline is controlled by exposures along the Sikanni Chief River, which cuts down into D_s dolostone in the core of this anticline, but not to the level of its transporting thrust. Other footwall structures are only roughly delineated by outcrop. Both east and west of Camp anticline, footwall exposures of the D_{sp} limestone are consistently rich in amphoporoids, which indicates a stratigraphic position in the uppermost D_{sp} limestone. We infer that nonoutcropping MD_{br} shale fills the covered areas between these outcrops and the Mount Bertha thrust. Our interpretation shows a relatively planar Mount Bertha thrust that cuts both up- and downsection through second-order footwall structures, which indicates this part of the Mount Bertha thrust formed after these footwall structures.

There is no control on the footwall structural geometry within or below the D_{pp} do-

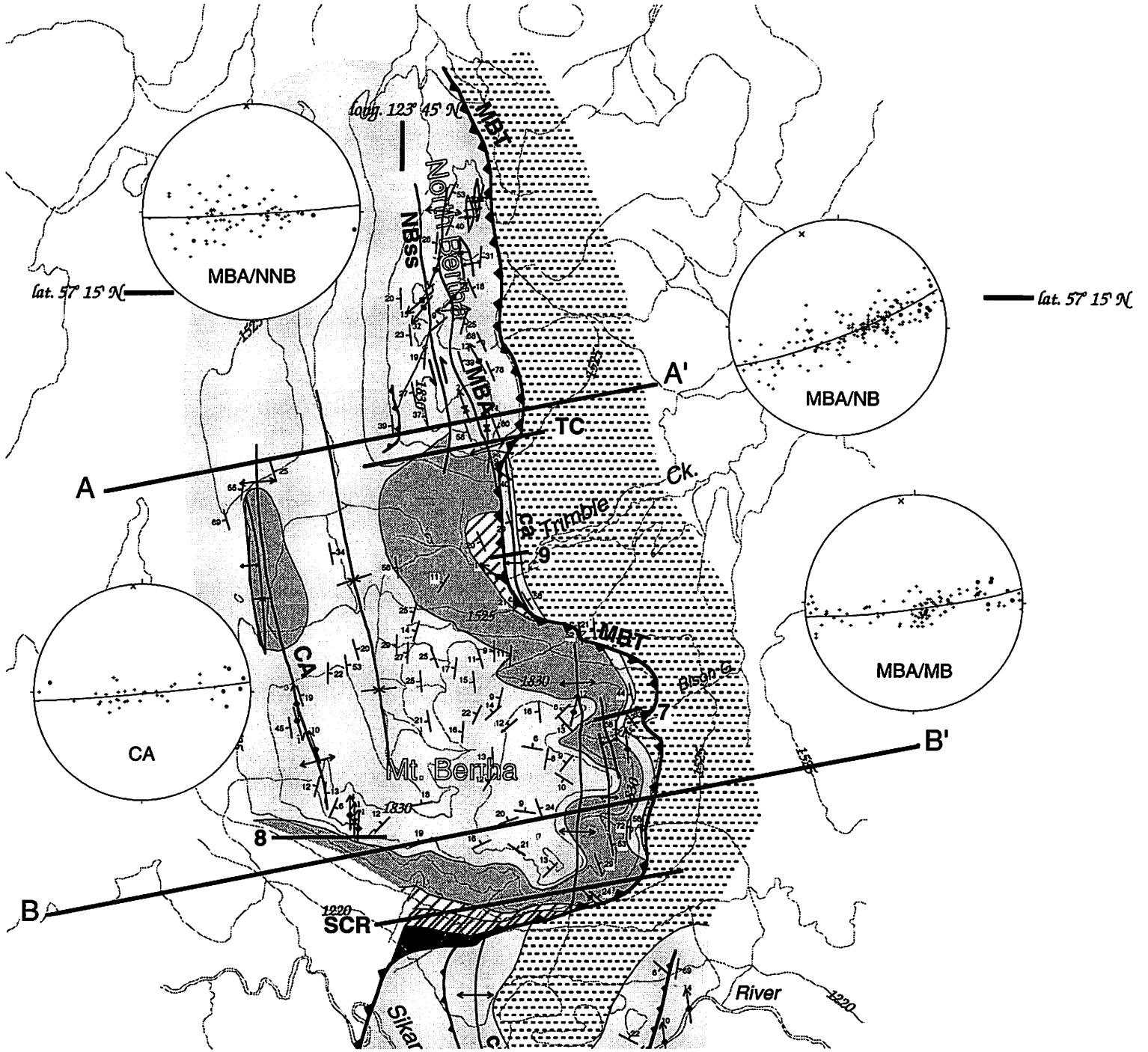

Figure 6. Geological map of the Mount Bertha study area. Only representative structural measurements are shown. Lines A–A′, B–B′, C–C′, and D–D′ are cross-section locations (see Fig. 10). SCR is line of Sikanni Chief River profile exposure (see Figs. 3A, 3B, 5A, and 15). TC is line of Trimble Creek profile exposure (see Figs. 3C, 3D, and 5B). 7, 8, and 9 indicate views shown in Figures 7, 8, and 9, respectively. MBA, Mount Bertha anticline; CA, Cranswick anticline; SA, Sidenius anticline; ca, Camp anticline; MBT, Mount Bertha thrust; NBss, North Bertha strike-slip fault. Equal-area stereograms show complete set of poles to bedding (+), cleavage (●), the best-fit great circle to bedding plus cleavage (the π-circle) and the π-pole (×). Indicated domains for stereograms are MBA/

NNB, data for Mount Bertha anticline for the northern one-third of North Bertha; MBA/NB, data for Mount Bertha anticline for the southern two-thirds of North Bertha; MBA/MB, data for Mount Bertha anticline for Mount Bertha; MBA/SB, data for Mount Bertha anticline for South Bertha; CA, data for Cranswick anticline. Note duplication where cut.

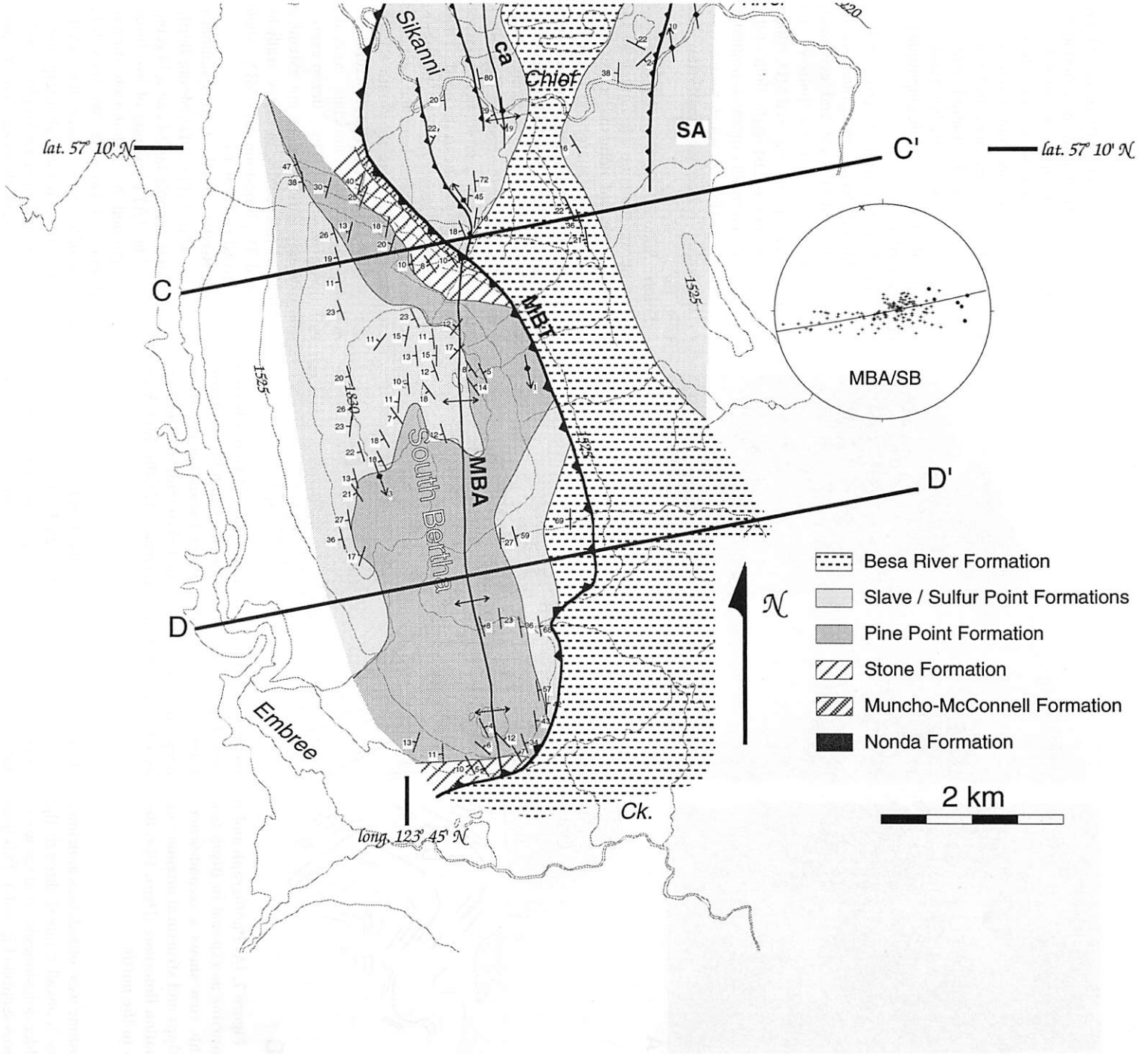

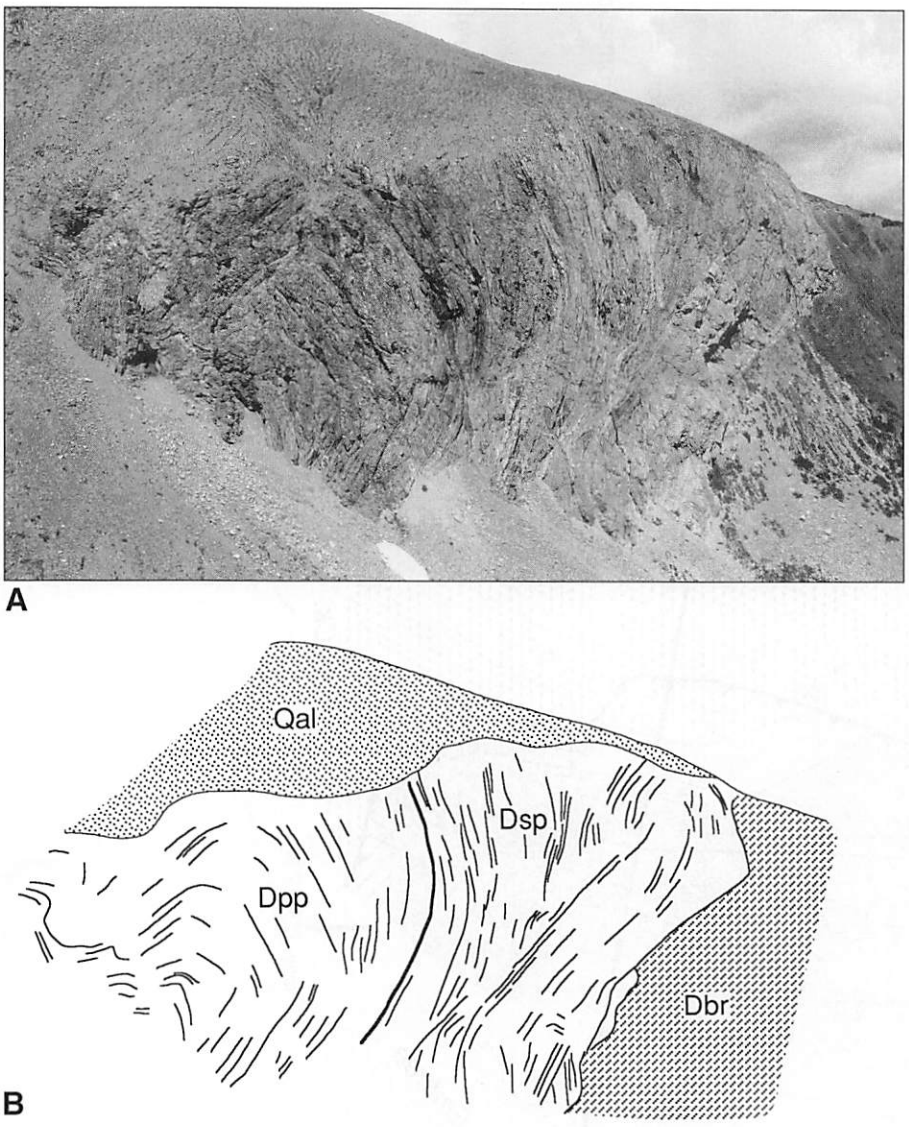

Figure 7. (A) Photograph and (B) line tracing of lower forelimb region of Mount Bertha anticline as exposed in Bison Gully, east slope of Mount Bertha (see Fig. 6 for location). This view shows a second-order fold developed in the Pine Point Formation dolostone (Dpp) and structural attenuation in steeply dipping to overturned Slave/Sulfur Point Formation limestone (Dsp). Dbr, Besa River Formation; Qal, Quaternary (?) alluvium. View is to the north.

lostone west of Sidenius anticline. We place the footwall ramp(s) through the D_{pp} and older dolostones beyond the west end of our cross section (Fig. 10B). This interpretation is forced by the contractional structures observed in the D_{sp} limestone throughout the footwall; the ramp in the D_{pp} dolostone must be west of the restored west end of these D_{sp} limestone structures. Our interpretation indicates a minimum displacement on the Mount Bertha thrust of ~5 km at the top of the D_{pp} dolostone.

North Bertha (A–A′). The line of this section (Fig. 10A) passes through Mount Bertha anticline near the Trimble Creek profile exposure and through Cranswick anticline at the position of its maximum amplitude (see Fig. 6). The lower limit of control for this section is ~1400 m elevation (base level of the Trimble Creek drainage). Details of the second-order structures within Mount Bertha anticline are not shown at the scale of these cross sections, but they are similar here to those observed in the Trimble Creek profile section (Fig. 5B).

Cranswick anticline is interpreted to be a fault-bend fold modified by a second-order forethrust, back thrust, and associated fault-propagation folding (Fig. 10A). The Mount Bertha thrust cuts laterally upsection in the hanging wall between the Central Bertha and North Bertha cross sections beneath Mount Bertha anticline, but it stays flat in the upper S_n dolostone beneath Cranswick anticline. As a result, the ramp height associated with Cranswick anticline (and, consequently, the fault-bend fold amplitude) increases northward.

North of the North Bertha cross section, both the Mount Bertha and Cranswick anticlines plunge northward and eventually lose definition (beyond the limits of our mapping) in the poorly exposed MD_{br} shale. Sidenius anticline is east of the limit of this cross section. Footwall outcrop is limited to Camp anticline (Fig. 9), which we interpret to be within a footwall imbricate slice (Fig. 10A).

South Sikanni (C–C′). Outcrops of Mount Bertha anticline are limited to the backlimb of the fold along this cross section (see Fig. 6). The geometry and position of the fold crest are determined by projection of surface data from a few kilometers to the south. The backlimb has a maximum dip of ~20° in the line of this section (Fig. 10C), but backlimb dips of over 40° are measured within 1 km along strike to the north. These steeper dips are probably the southernmost vestiges of Cranswick anticline, which is completely absent from the South Sikanni cross section (Fig. 10C). The structural culmination of Sidenius anticline coincides with this cross section. The outcrop expression of Camp anticline does not extend as far south as this section, but structurally intercalated D_{sp} limestone and MD_{br} shale are observed (see Fig. 6).

South Bertha (D–D′). In this southernmost cross section (Fig. 10D), Mount Bertha anticline has a simple fault-bend fold geometry (see Fig. 1A) consisting of two broad hinges separated by a uniformly dipping central limb, ~1 km wide. We have little direct data of footwall structure through this region (Fig. 6). Our footwall interpretation is based on map data of Taylor (1979) within the Embree Creek drainage and the footwall geometry observed in cross sections to the north.

THE MOUNT BERTHA THRUST

Structure-contour and hanging-wall-cutoff maps of the Mount Bertha thrust (Fig. 11) have been generated using the mapped trace of the Mount Bertha thrust (Fig. 6) and the series of cross-section in-

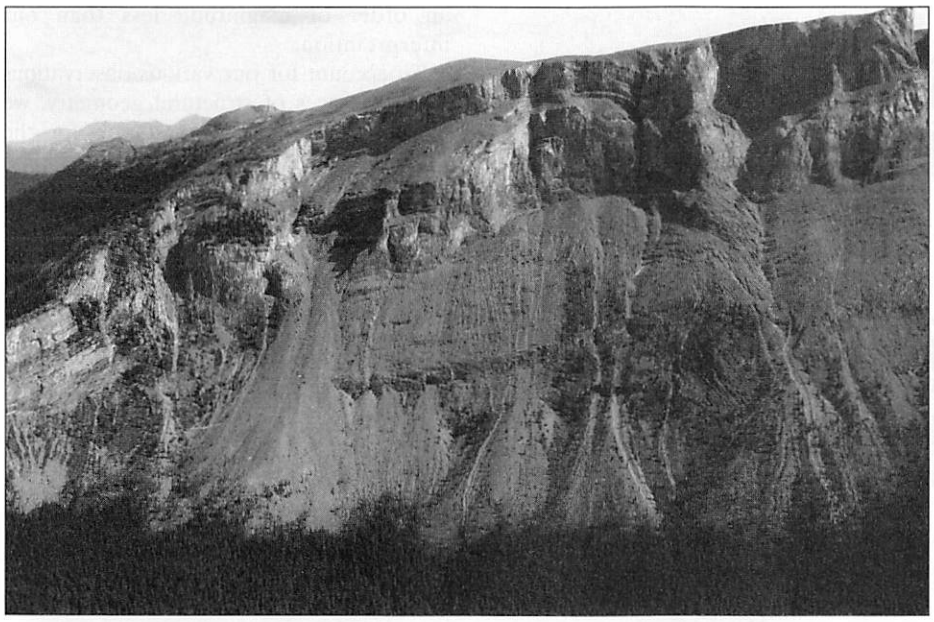

Figure 8. Cranswick anticline, a low-amplitude box fold on the south slope of Mount Bertha (see Fig. 6 for location). View is to the north.

terpretations of the Mount Bertha structure (Fig. 10). The structure-contour map (Fig. 11A) indicates the present fault configuration, which is the product of initial footwall fault geometry and subsequent modification of the fault surface. In contrast, the hanging-wall-cutoff map (Fig. 11B) reflects the hanging-wall fault configuration at its earliest stages of displacement.

Excepting the region between cross sections C–C′ and B–B′ (i.e., across the Sikanni Chief River drainage), the fault-surface structure contours have a general trend of 350° to 360° (Fig. 11A), which coincides with the general fold axis trend of both Mount Bertha and Cranswick anticlines. The fault surface has a relatively gentle westward dip (8° to 12°) beneath the core region of Mount Bertha anticline through Mount Bertha and South Bertha, increasing westward (to 20° to 30°). The fault has a comparatively steep westward dip (~35°) along the length of North Bertha, but then flattens westward beneath the forelimb of Cranswick anticline. The overall map-view curvature of the structure contours through the map area (Fig. 11A) indicates a broad scooped-shape fault morphology, with a trough near the southern end of Mount Bertha and a ridge near cross section C–C′.

The hanging-wall-cutoff map (Fig. 11B) shows the formation in the hanging wall that is in contact with the Mount Bertha thrust. Boundaries of the various formations on this map correspond to hanging-wall cutoff positions. Locations of the hanging-wall ramp hinges are also shown on this map. A single ramp is preserved south of the Sikanni Chief River drainage. North of this drainage there are two distinct ramps. They are quite close together in the Sikanni Chief River profile section (Fig. 5A), but become more widely separated northward.

An oblique ramp associated with Mount Bertha anticline is indicated on the hanging-wall-cutoff map by the nonparallelism between formation cutoffs and the lower ramp hinge underlying this fold (Fig. 11B). The incipient fault geometry was broadly scoop-shaped, with a trough that approximately coincides with the Sikanni Chief River profile section. The ramp that created Mount Bertha anticline cut obliquely upsection both north and south from this location.

Several features on both of these fault-surface maps appear to have some relationship to the Sikanni Chief River drainage. For example, a swing in the structure contours (Fig. 11A) and the split of the hanging-wall ramps both occur at this location. The troughs of both the incipient Mount Bertha thrust fault surface (Fig. 11B) and the present fault surface (Fig. 11A) lie just north of this drainage. The apparent correspondence of these several features may be a coincidence, or it may indicate the presence and influence of some deep structural feature aligned with the Sikanni Chief River. We lack subsurface data to verify and identify this inferred deep-seated feature.

FOLD-THRUST EVOLUTION

Within the spectrum of fault-bend, fault-propagation, and detachment folds, the only fold-thrust style that will yield a broad fold geometry in a competent stratigraphic section, as seen in the Sikanni Chief River profile exposure (Figs. 3A, 3B, and 5A) and in the southern three cross sections (Figs. 10B,

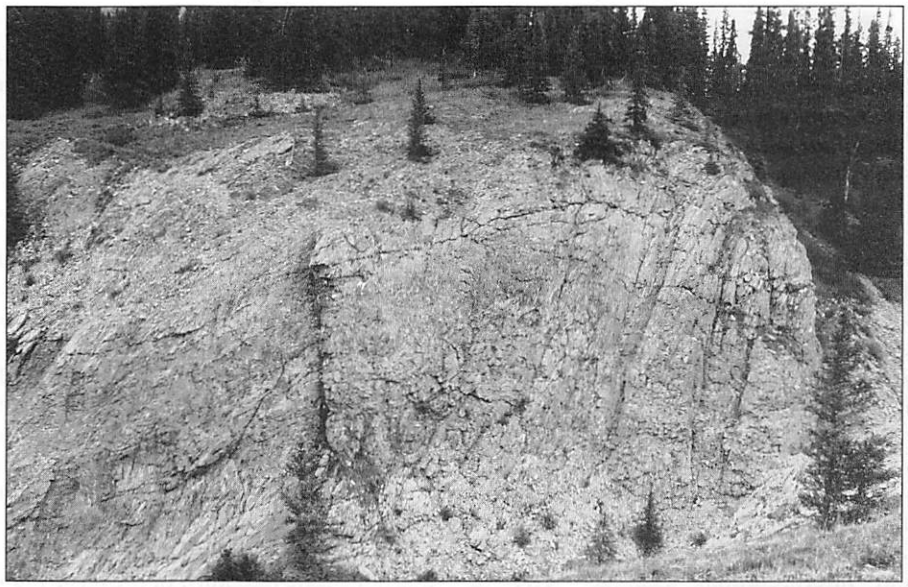

Figure 9. Camp anticline developed in Slave/Sulfur Point Formation in the footwall of Mount Bertha thrust along Trimble Creek. Note strong axial-planar cleavage (see Fig. 6 for location). View is to the north.

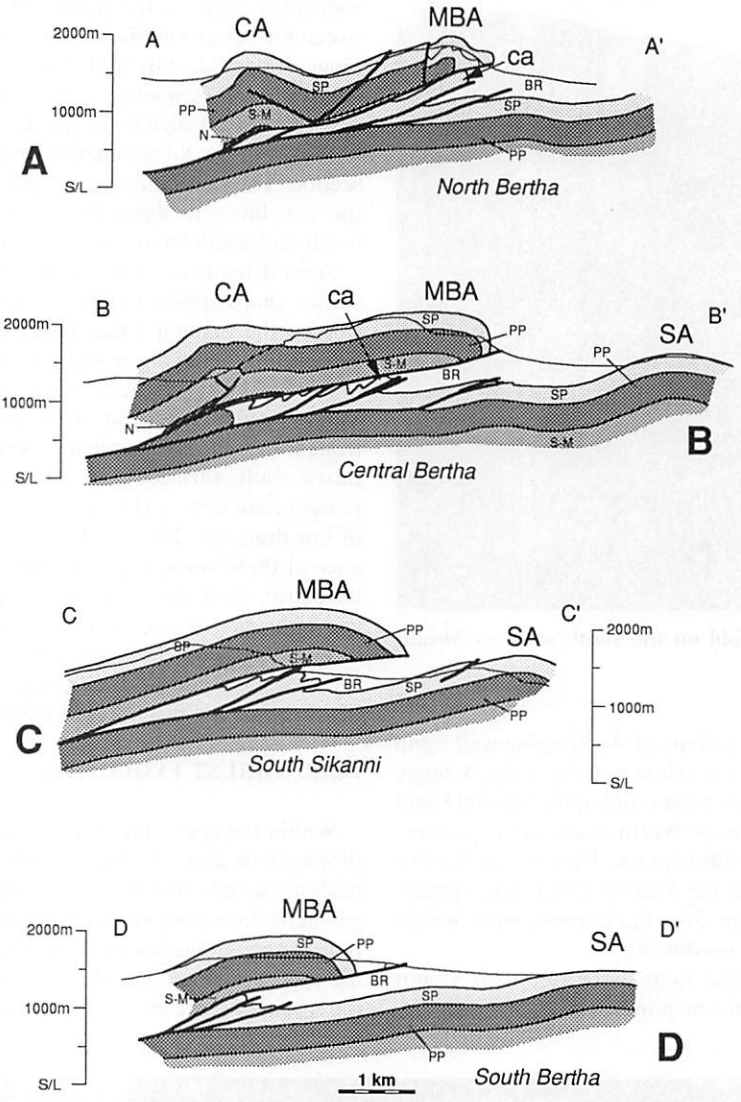

Figure 10. Cross-section interpretations of the Mount Bertha structure. Lines of section identified in Figures 6 and 11. BR, Besa River Formation; SP, Slave/Sulfur Point Formation; PP, Pine Point Formation; S-M, Stone and Muncho-McConnell formations; N, Nonda Formation; MBA, Mount Bertha anticline; CA, Cranswick anticline; SA, Sidenius anticline; ca, Camp anticline.

10C, and 10D), is the fault-bend fold (Fig. 1A). Fault-propagation folds inherently have a tighter fold geometry, and detachment folds can develop this broad fold geometry only if a thick sequence of relatively ductile material is available to flow into the core of the fold (Jamison, 1987), which is not observed here.

Several aspects of the Mount Bertha structure, though, are inconsistent, to varying degrees, with a strict fault-bend fold interpretation. The geometry of Mount Bertha anticline on North Bertha (Figs. 3C, 3D, and 5B) is much more complex than is suggested by the basic fault-bend fold model (see Fig. 1). The development of extensive deformation in the footwall region in advance of the thrust, as indicated by structures in the Sikanni Chief River drainage region (see Fig. 10B) is also not characteristic of the Rich/fault-bend fold model (Suppe, 1983). In our cross section interpretations (Fig. 10), dip separation of the hanging-wall and footwall cutoffs at the top of the D_{sp} limestone (~2 km) is much less than at the top of the D_{pp} dolostone (>5 km). In the basic fault-bend fold model (Suppe, 1983), the difference in dip separation at these two levels should be no more than ~300 m, an order of magnitude less than our interpretation.

To account for our various observations and inferences of structural geometry, we offer a fold-thrust interpretation for the Mount Bertha structures that is based upon the fault-bend fold model (see Fig. 1) but includes, locally, a hinterland deformational sequence and varying contributions of detachment and fault-propagation folding.

Mount Bertha Anticline

Fault ramp formation preceded any significant macroscale folding within the dolostone units of these units. The Mount Bertha thrust simply cut upsection along one or two thrust ramps (*r* and *s* in Fig. 12A) to an upper flat at or near the base of the D_{sp} limestone. A fault-bend fold (Fig. 1A) developed as the hanging-wall section moved toward the foreland over each footwall ramp (Fig. 12B). In the early phases of fault movement, the Mount Bertha thrust died out into a series of detachment or lift-off folds in the D_{sp} limestone (Fig. 12B). Eventually, the main fault began to break back through the limestone folds (Fig. 12C). This produced a trailing imbricate fan (Boyer and Elliott, 1982) in the D_{sp} limestone folds and created thrust ramp(s) *t*, which connects to a thrust flat at some horizon well up in the MD_{br} shale (Fig. 12D).

Our scenario for fold-thrust development to this stage is similar to one proposed by Thompson (1981), with the important difference that Thompson (1981) indicated the fault-tip folding occurs in the MD_{br} shale and does not involve the underlying carbonate rocks. Thompson (1981) suggested that the change in deformational style is fostered by the contrast in mechanical characteristics between the carbonate and shale units. Whereas we agree with the general model and concepts of Thompson (1981), our observations indicate that the contrast in mechanical characteristics between dolostone and limestone is the more significant factor in the fold-thrust development of the Mount Bertha structure.

The structural geometry of Mount Bertha anticline was altered during progressive foreland movement of the hanging-wall structure according to the composition of the involved mechanical-stratigraphic sequence. Where the thickness of the lower dolostone mechanical stratigraphic unit (see Fig. 4) within the core of the fold is >~100 m (e.g., Figs. 10B, 10C, and 10D), it has provided a relatively rigid core to the anticlinal

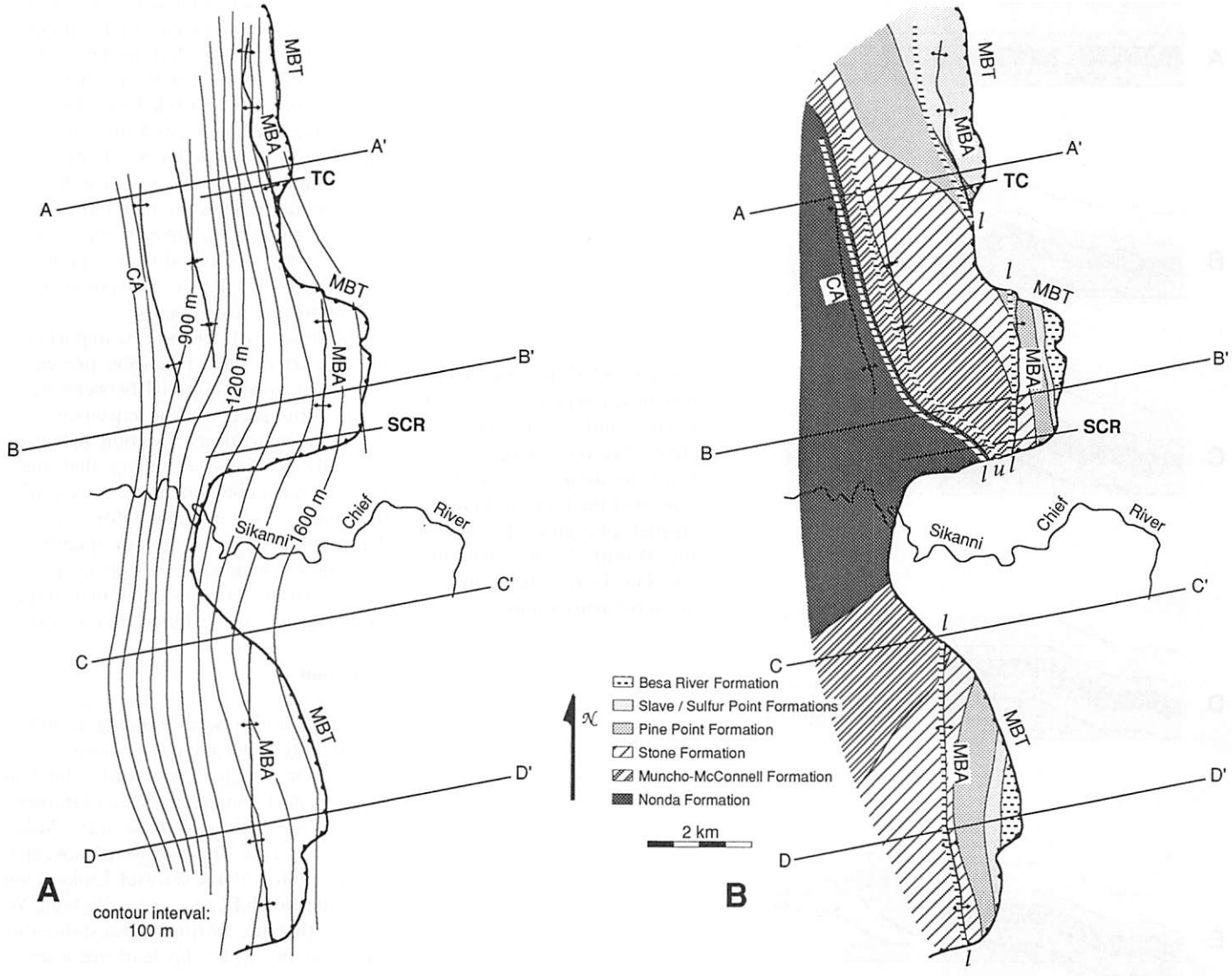

Figure 11. (A) Structure-contour map and (B) hanging-wall-cutoff map of the Mount Bertha thrust surface. The variable spacing between the fault-surface structure contours in A reflects changes in the dip of the fault surface. Lines A–A′, B–B′, C–C′, and D–D′ are cross-section locations (see Fig. 10). SCR is line of Sikanni Chief River profile exposure (see Figs. 3A, 3B, 5A, and 15). TC is line of Trimble Creek profile exposure (see Figs. 3C, 3D, and 5B). MBA, surface location of Mount Bertha anticline; CA, surface location of Cranswick anticline; MBT, trace of Mount Bertha thrust. Narrow, horizontally striped zones on B indicate location of hanging-wall ramp hinges, where *l* and *u* indicate upper and lower ramp hinges, respectively.

structure. Some second-order folding and faulting occurred in these relatively massive dolostone units, but the macroscale structural geometry was altered very little. D_{pp} dolostone and, especially, D_{sp} limestone, though, were faulted and/or tectonically attenuated in the forelimb region and overridden during advance of the thrust sheet (see Figs. 5A and 12D).

Where the lower dolostone mechanical stratigraphic unit is thin or absent in the core of the fold, as in the northern part of the study area (see Figs. 5B, 10A, and 11B), the structural geometry of Mount Bertha anticline is dominated by second-order contractional structures (detachment/lift-off folds, forethrusts, backthrusts, and fault-propagation folds) developed within the D_{sp} limestone and D_{pp} dolostone. Some of these second-order structures may have developed at the tip of the evolving Mount Bertha thrust (Fig. 12B), but others are probably associated with hanging-wall advance.

Cranswick Anticline

Cranswick anticline initiated as a fault-bend fold above the western thrust ramp through the dolostone units (*r* in Fig. 12). This fold geometry was significantly modified and amplified by fault-propagation folding associated with second-order forethrusts and back thrusts in the core of the fold (Figs. 10A, 10B, and 12E). These second-order thrusts probably developed during the final stages of movement on Mount Bertha thrust, after fault movement on the foreland side of ramp *t* (Fig. 12) had ceased. It evidently became easier to produce new deformation at this inflection in the fault surface than to move the hanging wall through this zone and the footwall flat to the east. An

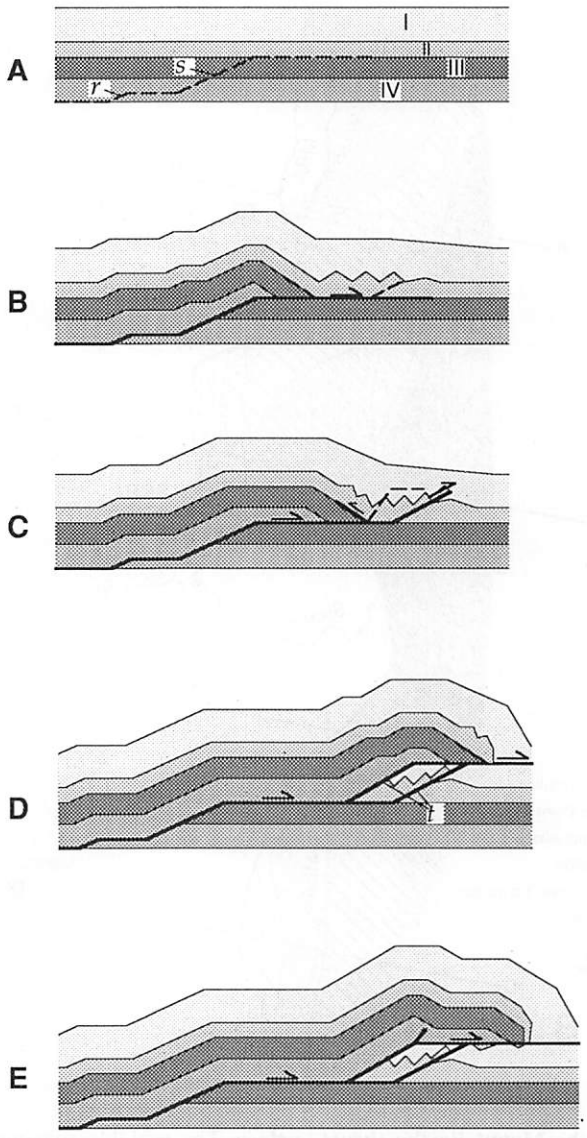

Figure 12. General model for fold-thrust evolution of Mount Bertha and Cranswick anticlines. See text for discussion. Units are designated I to IV to represent the four mechanical-stratigraphic units observed on the Mount Bertha structure (see Fig. 4); *r*, *s*, and *t* identify discrete thrust ramps.

identical model of late, second-order fault-propagation folding above a footwall upper ramp hinge was proposed by Mitra (1990) for Dry Horse Springs anticline in the Absaroka thrust sheet in Wyoming (Lamerson, 1982). Note that the second-order back thrust in the core of Mount Bertha anticline in the Trimble Creek profile similarly emanates from an inflection in the Mount Bertha thrust (Fig. 5B).

DETRUSION AND EXTRUSION

Detrusion

In our examination of the Mount Bertha structure we observe repeated indications that the D_{sp} limestone has been or was in the process of being removed from the lower forelimb region of the hanging-wall structure. This is accomplished by a combination of break-back thrusting and delamination of overturned and attenuated beds (Fig. 13). This process was continuous through, at least, the last 2 km of movement on the Mount Bertha thrust, for we observe a continuous zone of overridden D_{sp} limestone that extends along the fault contact for 2 km in the transport direction in the Sikanni Chief River profile exposure.

We term this process *detrusion* (from the verb *detrude*, meaning "to force down"), in reference to our interpretation that the lower forelimb material is being forced down from the hanging wall into the footwall by the advancing thrust sheet. Along the Sikanni Chief River profile exposure, the D_{sp} limestone pods along the fault zone have been cataclastized at the contact with the hanging-wall dolostone units (along the Mount Bertha thrust) but display no shear fabric at the contact with the underlying MD_{br} shale. The detruded D_{sp} limestone pods have been impressed into the shale. They are not horse blocks, because the lower bounding surface is not a fault. In other circumstances, the material removed from the hanging wall may be incorporated into true horse blocks along the fault zone (e.g., Serra, 1977; Knipe, 1985) or into footwall imbricate thrust sheets.

The process of detrusion is important in the context of most balancing procedures because it moves material between neighboring thrust sheets during movement along the intervening thrust. Section balance is generally evaluated assuming that major fault-bounded components of rock contain the same mass of material before and after deformation. If a significant quantity of hanging-wall material is detruded, a geologically accurate cross section may appear "unbalanced" and be difficult to reconstruct.

Extrusion

The north-northwest–trending second-order folds that developed on North Bertha east of the North Bertha strike-slip fault suggest a northward component of transport that is not evident elsewhere in the Mount Bertha structure. This northward movement is compatible with the sinistral displacement along the North Bertha strike-slip fault. We suggest that the north-northwest–trending folds and the strike-slip fault are a linked system of structures developed in association with lateral displacement, or tectonic extrusion, that accompanied the general eastward transport of the Mount Bertha structure.

The North Bertha strike-slip fault defines the western boundary of the region with lateral displacement. It produces a well-defined lineament along the length of North Bertha, but does not extend across the Trimble Creek drainage. The width of the Trimble Creek valley (~1.5 km) places an upper limit on the magnitude of strike slip on this fault, but the actual strike displacement is probably much less than this.

Apotria et al. (1992) suggested that an oblique thrust ramp can produce a component of lateral displacement in the overlying thrust sheet. The hanging-wall-cutoff map of the Mount Bertha thrust (Fig. 11) indicates the hanging-wall ramp cuts upsection to the north in the vicinity of the Trimble Creek

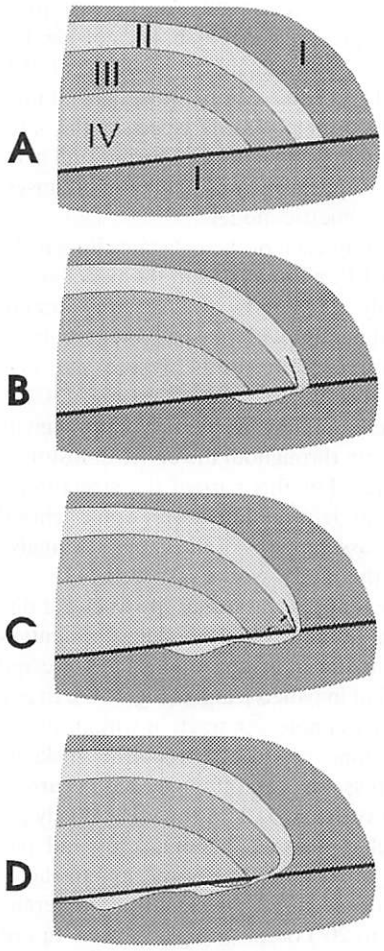

Figure 13. Schematic diagrams of the progressive (A to B to C to D) structural transfer of rock from the lower forelimb to the footwall (detrusion), subjacent to the thrust surface, by a combination of penetrative attenuation and second-order faulting. Units are designated I to IV to represent the four mechanical-stratigraphic units observed on the Mount Bertha structure (see Fig. 4). Detrusion of a particular unit does not require detrusion of stratigraphically bounding units. Advance of the hanging wall may smooth second-order irregularities of the fault surface resulting from detrusion processes. The lower surface of detruded material may or may not be a fault surface.

drainage. The models of Apotria et al. (1992) predict an associated southward component of motion for the hanging-wall material in this situation, the opposite of our observations. We do not have an alternative explanation for the northward component of displacement of this segment of the Mount Bertha structure.

The phenomenon of lateral extrusion would obviously violate the basic assumption of two-dimensional (2-D) balancing procedures. In the case of the North Bertha structures, where the associated strike-slip fault is normal to the transport direction, the amount of material moving out of a regional profile section would be roughly equivalent to the material moving into the section. In this case, the lateral movement would have little effect on the 2-D balance of the structure.

GEOMETRIC ANALYSIS OF MOUNT BERTHA ANTICLINE

The Sikanni Chief River profile section of Mount Bertha anticline (Fig. 5A) provides the opportunity to critically evaluate the geometric models that relate the *fold* geometry of a fault-bend fold to the *fault* geometry (Figs. 14A and 14B; Suppe, 1983; Jamison, 1987). The fault-bend fold geometry is clearly defined within the dolostone units in this profile, and we infer that this part of the Mount Bertha structure has evolved strictly in accord with the fault-bend fold concept (compare Figs. 1A and 12B).

Comparison of the geometric model to observed fold geometry is made by superposing a geometric model composed of several constant-dip panels on the Sikanni Chief River profile section (Figs. 14C, 15A, and 15C). The western two constant-dip panels (panels a and b in Fig. 15) overlie the main hanging-wall flat of the Mount Bertha thrust, and the constant-dip panels to the east (panels c through i in Fig. 15) overlie the region of the hanging-wall ramps and secondary flat (see Fig. 5A). An initial geometric model (model A, Fig. 15A) has been constructed using constant unit thicknesses across the fold, as per the assumption of Suppe (1983). Formation thicknesses observed on the western side of the profile section (panel a of Fig. 15A) are assumed to represent their true stratigraphic thicknesses. Boundaries between most of the constant-dip panels in model A are chosen to coincide with discrete changes in the hanging-wall cutoff angle (δ) along the Mount Bertha thrust. Within each constant-dip panel over the ramp regions, values of t (the stratigraphic thickness truncated by the Mount Bertha thrust within the panel) and h (the length of the ramp within the panel) are used to determine this cutoff angle (see Fig. 14D):

$$\delta = \sin^{-1}(t/h) = 180° - \gamma$$

where γ is the fold interlimb angle (see Figs. 14A and 14B). δ minus fault dip is the bedding dip within the individual panels ($\delta = 0$ within panels a and b).

Model A agrees reasonably well with the true configuration of the fold (Fig. 15A). Except in panels h and i (see Fig. 15A), the dips within the individual panels of the model correspond favorably to those observed in the profile section. Formation boundaries in the profile section (solid lines in Fig. 15), however, consistently fall below the corresponding boundaries of the model (dashed lines in Fig. 15). This indicates that a general thinning of the carbonate units occurs across the fold structure. (The number of constant-dip panels used in the model graphic is an arbitrary choice. We have attempted to include enough panels to address the macroscopic detail of the fold structure. The use of more constant-dip panels does not significantly change the comparative fit between the model and the profile section.)

The geometric models of both Suppe (1983) and Jamison (1987) relate interlimb angle of a fault-bend fold (γ) to the original ramp angle (α). The value of γ can be determined directly from the profile section, but there is no direct control on α. Values of α for the individual dip panels may be inferred from the γ-α charts (Fig. 14B), which then allows a theoretical reconstruction of the original ramp configuration through the SD_m and D_s dolostone sequence (Fig. 15B). The reconstructed fault has two concave-upward segments through this interval, each having a maximum dip of ~25°.

To address the noted thinning through the fold structure, an alternative model has been constructed using the assumption of uniform structural thinning within each of the constant-dip panels (model B, Fig. 15C). Model B uses the same hanging-wall-ramp segments as the constant-unit-thickness model (Fig. 15A). In the western part of the fold, the δ-values of the individual panels of model B are determined using (1) the α-values derived from model A (Fig. 15B), (2) the α-γ charts (Fig. 14B), and (3) an iterated estimate of structural thinning. The resultant δ-values are slightly less than the corresponding values in model A, and the panel boundaries have shifted to accommodate the differential thinning between panels (these boundaries are determined using equation 7 in Jamison, 1987). Even a small variation in thickness between adjacent panels can produce an appreciable shift in the orientation and position of the panel boundary (compare Figs. 15A and 15C). De-

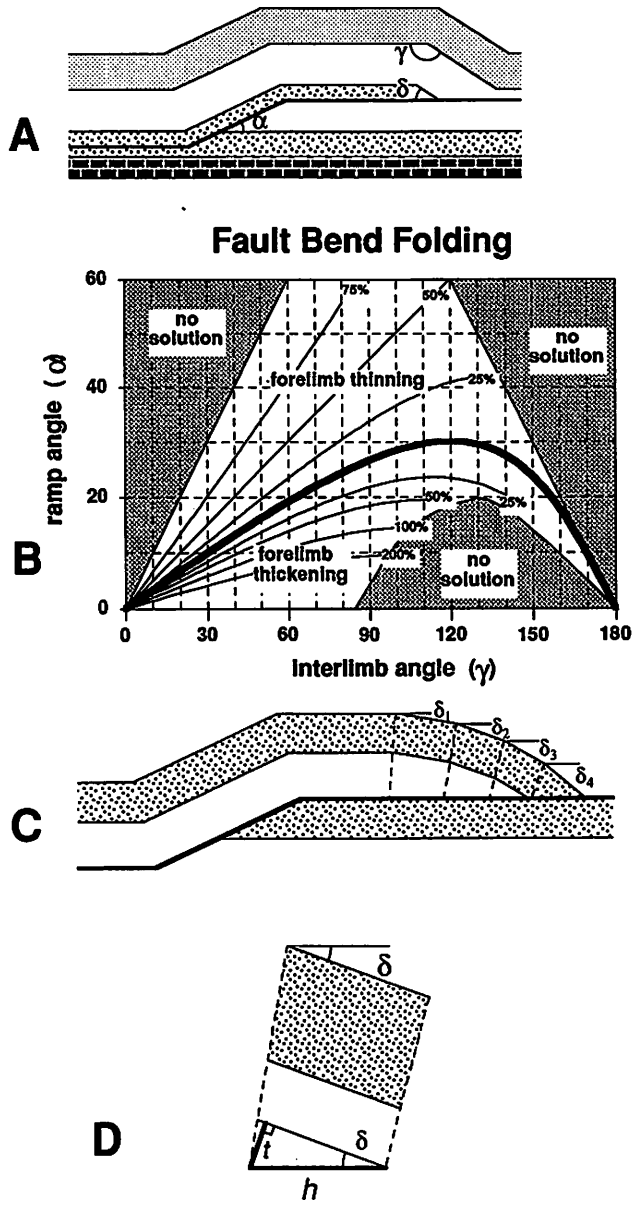

Figure 14. (A) Reference angles used for geometric analyses and construction of geometric models: α, ramp angle; γ, fold interlimb angle; δ, forelimb cutoff angle (which is equal to the forelimb dip for a horizontal fault). (B) Chart relating ramp angle to fold interlimb angle for a fault-bend fold with the indicated structural thickening or thinning of the fold forelimb (from Jamison, 1987). (C) The geometric model for the SCR profile (Fig. 15) is constructed using a suite of constant-dip panels, each having a specified cutoff angle (δ_i). (D) The value of δ for each constant-dip panel is calculated using the stratigraphic thickness (t) and the cutoff width (h) of the beds truncated at the fault surface within the panel. See text for equation.

trusion of forelimb material in the eastern part of the profile section can produce unreliable calculated α-values. Through this region, model B (Fig. 15C) was constructed using the δ-values from model A (Fig. 15A).

The fit between model B and the profile section is extremely good in the western part of the profile section (panels a, b, c, and d of Fig. 15C): Observed bedding orientations are within a few degrees of model δ-values, and formation boundaries fall within a few meters of model predictions. In the central part of the structure, above the secondary hanging-wall flat (panels e and f of Fig. 15C), the fit between model B and the profile section is a bit rougher, though still reasonable. In the eastern part of the profile (panels g, h, and i of Fig. 15C), there are serious misfits at the level of D_{sp} and D_{pp}. These comparative fits and misfits can be used to identify aspects of the natural deformation that are compatible and in conflict, respectively, with the basic premises of the geometric models.

Within each of the constant-dip panels in model B, all units within the panel are uniformly thinned by the specified amount. Bedding dips within each panel are, by definition, constant. In the western part of the fold (panels a, b, c, and d of Fig. 15C), observed thinning is, in fact, approximately uniform throughout the entire dolostone sequence. For this part of the structure, the natural deformation closely approaches the basic assumptions of the geometric analysis, and the model works very well.

In contrast, variations in structural thickening/thinning and bedding orientation within the individual dip panels are quite evident in panels e and f (Fig. 15C). In panel e, for example, contraction within the SD_m dolostone produced structural thickening, whereas structural thinning has occurred in the overlying D_s dolostone. Relatively good matches between bedding dips and panel dips of model B are found low in the carbonate section, but significant differences (15° to 20°) occur at higher levels. In order to match such details of the structural geometry, a model would have to allow vertical as well as lateral variations in unit thickness and bedding dip.

The geometric model approaches of Suppe (1983) and Jamison (1987) assume that major thrust faults define domains of constant material volume. As discussed above, the process of detrusion conflicts with this assumption. As a result, the models show very poor agreement with the true structural geometry in the areas affected by detrusion (the upper part of the carbonate sequence in panels g, h, and i in Fig. 15C). In a positive sense, the misfit between the model geometry and the profile section should be a measure of how much material has been detruded.

This analysis has been conducted assuming that the thinning of the various carbonate units through the fold is structural rather than stratigraphic. We cannot eliminate the possibility that the thickness variations are, in fact, stratigraphic. It would be remarkably coincidental, however, that the percent thickness changes are similar in each of the dolostone formations and that these thick-

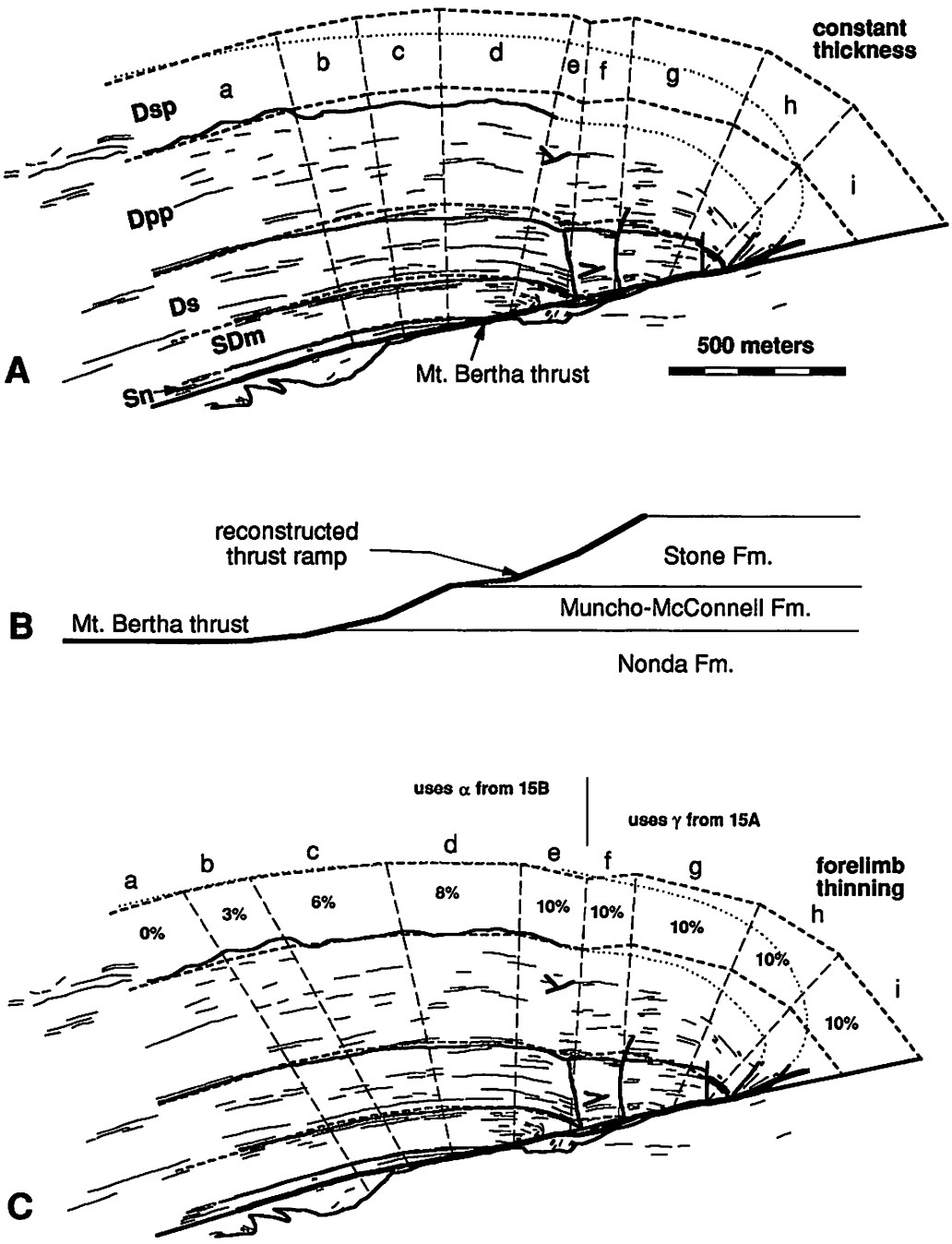

Figure 15. (A) Constant-bed-thickness geometric model fit to Sikanni Chief River profile section of Mount Bertha anticline (see Fig. 5A). See Figure 4 for formation abbreviations. (B) Reconstructed footwall-ramp geometry of the Mount Bertha thrust through the lower dolostone mechanical-stratigraphic unit within the Sikanni Chief River profile section. (C) Geometric model fit to SCR profile section of Mount Bertha anticline based on structural thinning, by the indicated percentage, within the various constant-dip panels. See text for discussion.

ness variations correspond so directly to structural geometry.

Meso- to microscale deformational features in the dolostones consist of extension fractures (predominantly oriented at high angles to S_0) and pressure solution seams (most oriented parallel to S_0). The S_0-parallel pressure solution seams are the only features properly oriented to produce the inferred structural thinning. Although these may be, in part, burial diagenesis features, fracture-offsetting relationships indicate syn- to post-tectonic pressure solution activity as well. We have not attempted to quantify the thinning produced by the pressure solution features.

CONCLUSIONS

Mount Bertha anticline and its companion structure, Cranswick anticline, are fundamentally fault-bend folds. The geometries of these structures have been modified from the classic Rich (1934) configuration by superposed components of fault-propagation folding and detachment/lift-off folding and by detrusion of lower forelimb material. Significant variations in structural configuration are evident along strike, and even at different stratigraphic levels within a single profile section.

The macroscale deformational processes and the resultant structural geometries are fundamentally dictated by the individual and composite deformational characteristics of the involved mechanical-stratigraphic

units. The 900+-m-thick sequence of middle Paleozoic carbonate rocks that forms the core of the Mount Bertha structure contains threeimportantanddistinctmechanical-stratigraphic units: a lower, massive dolostone unit (up to 370 m thick), a middle, bedded dolostone (325 m thick), and an upper limestone unit (220 m thick). The contrast in deformational character between the limestone and the dolostone units is quite dramatic, and the mechanical contrast between the two dolostone units also results in significant differences in structural geometries.

Where the lower dolostone mechanical-stratigraphic unit in the hanging wall is over ~100 m thick, Mount Bertha anticline displays the classic shape of a mode I fault-bend fold (Suppe, 1983). The involvement of this mechanically competent unit in the core of the structure favors both the initial occurrence of the fault-bend fold style and the retention of this simple fold geometry during transport of the hanging-wall structure. An oblique ramp in the Mount Bertha thrust results in a diminished thickness of this sequence in the hanging wall along strike. Where it is thin or absent in the core of the fold, second-order contractional structures develop in the upper dolostone and limestone mechanical-stratigraphic units. These second-order features consist predominantly of fault-propagation folds (in the dolostone) and detachment/lift-off folds (in the limestone). They formed both during initial fault propagation and through subsequent hanging-wall transport. These second-order structures locally dominate the structural geometry of Mount Bertha anticline.

During transport of the hanging-wall structure, the lower forelimb regions of folds in the upper two mechanical stratigraphic units have been detruded from the hanging wall into the footwall adjacent to the thrust. Detrusion of the limestone unit was a continuous process associated with fold transport.

A survey-controlled profile section of the fault-bend fold geometry in the central part of Mount Bertha anticline has been used to critically evaluate geometric models for fault-bend folding (Suppe, 1983; Jamison, 1987). For Mount Bertha anticline, it is demonstrated that an assumption of constant bed thickness across the fold is not appropriate. A model that allows for structural thinning provides a good match to the Mount Bertha structure, except through the parts of the structure that have been subjected to detrusion. The mismatch between the model and the natural structure in the latter region may provide a measure of the amount of material that has been tectonically removed.

ACKNOWLEDGMENTS

This study was made possible through a research grant and logistical support from Amoco Canada Petroleum Co. Ltd. and a National Sciences and Engineering Research Council of Canada (NSERC) operating grant to the senior author. We would like to thank Gregg Erickson, Peter Cawood, Jeroen Van Gool, David Ferrill, Deborah Spratt, and Arthur Sylvester for their constructive reviews of early versions of the manuscript.

REFERENCES CITED

Al Saffar, M., 1993, Geometry of fault-propagation folds: Methods and applications: Tectonophysics, v. 223, p. 363–380.

Apotria, T. G., Snedden, W. T., Spang, J. H., and Wiltschko, D. V., 1992, Kinematic models of deformation at an oblique ramp, *in* McClay, K. R., ed., Thrust tectonics: London, Chapman and Hall, p. 141–154.

Bally, A. W., Gordy, P. L., and Stewart, G. A., 1966, Structure, seismic data and orogenic evolution of southern Canadian Rocky Mountains: Bulletin of Canadian Petroleum Geologists, v. 14, p. 337–381.

Bamber, E. W., Taylor, G. C., and Procter, R. M., 1968, Carboniferous and Permian stratigraphy of northeastern British Columbia: Geological Survey of Canada Paper 68-15, 25 p.

Boyer, S. E., and Elliott, D., 1982, Thrust systems: American Association of Petroleum Geologists Bulletin, v. 66, p. 1196–1230.

Chester, J. S., and Chester, F. M., 1990, Fault-propagation folds above thrusts with constant dip: Journal of Structural Geology, v. 12, p. 903–910.

Dixon, J. S., 1982, Regional structural synthesis, Wyoming salient of western overthrust belt: American Association of Petroleum Geologists Bulletin, v. 66, p. 1560–1580.

Faill, R. T., 1973, Kink-band folding, Valley and Ridge province, Pennsylvania: Geological Society of America Bulletin, v. 84, p. 1289–1314.

Jamison, W. R., 1987, Geometric analysis of fold development in overthrust terranes: Journal of Structural Geology, v. 9, p. 207–219.

Knipe, R. J., 1985, Footwall geometry and the rheology of thrust sheets: Journal of Structural Geology, v. 7, p. 1–10.

Lamerson, P. R., 1982, The Fossil Basin area and its relationship to the Absaroka thrust fault system, *in* Powers, R. B., ed., Geologic studies of the Cordilleran thrust belt: Denver, Colorado, Rocky Mountain Association of Geologists, p. 279–340.

Mitra, S., 1990, Fault-propagation folds: Geometry, kinematic evolution, and hydrocarbon traps: American Association of Petroleum Geologists Bulletin, v. 74, p. 921–945.

Rich, J. L., 1934, Mechanics of low-angle overthrust faulting as illustrated by Cumberland thrust block, Virginia, Kentucky, Tennessee: American Association of Petroleum Geologists Bulletin, v. 18, p. 1584–1596.

Serra, S., 1977, Styles of deformation in the ramp regions of overthrust faults: Wyoming Geological Association Guidebook, 29th Field Conference, p. 487–498.

Suppe, J., 1980, A retrodeformable cross section of northern Taiwan: Proceedings of the Geological Society of China, no. 23, p. 46–55.

Suppe, J., 1983, Geometry and kinematics of fault-bend folding: American Journal of Science, v. 283, p. 684–721.

Suppe, J., and Medwedeff, D. A., 1990, Geometry and kinematics of fault-propagation folding: Eclogae Geologicae Helvetiae, v. 83, p. 409–454.

Taylor, G. C., 1979, Trutch (94G) and Ware east half (94F, E1/2) map areas, northeastern British Columbia: Geological Survey of Canada Open File Report 606.

Taylor, G. C., and MacKenzie, W. S., 1970, Devonian stratigraphy of northeastern British Columbia: Geological Survey of Canada Bulletin 186, 62 p.

Thompson, R. I., 1981, The nature and significance of large "blind" thrusts within the northern Rocky Mountains, British Columbia, Canada, *in* McClay, K. R., and Price, N. J., eds., Thrust and nappe tectonics: Geological Society of London, p. 449–462.

Thompson, R. I., 1989, Stratigraphy, tectonic evolution and structural analysis of the Halfway River map area (94 B), northern Rocky Mountains, British Columbia: Geological Survey of Canada Memoir 425, 119 p.

Willis, B., 1890, Mechanics of Appalachian structure: U.S. Geological Survey 13th Annual Report, part II, p. 211–281.

MANUSCRIPT RECEIVED BY THE SOCIETY SEPTEMBER 2, 1994
REVISED MANUSCRIPT RECEIVED APRIL 20, 1995
MANUSCRIPT ACCEPTED AUGUST 18, 1995

Printed in U.S.A.